Adhesion G-protein coupled receptor 56 is required for 3T3-L1 adipogenesis

Al Hasan, Mohammad; Roy, Poornima; Dolan, Sharron; Martin, Patricia E.; Patterson, Steven; Bartholomew, Chris

Published in:
Journal of Cellular Physiology

DOI:
10.1002/jcp.29079

Publication date:
2020

Document Version
Author accepted manuscript

Adhesion G-Protein Coupled Receptor 56 is required for 3T3-L1 Adipogenesis

Authors: Mohammad Al Hasan, Poornima Roy, Sharron Dolan, Patricia E Martin, Steven Patterson and Chris Bartholomew.

Running title: Gpr56 regulates adipogenesis

Address: Department of Biological & Biomedical Sciences, School of Health & Life Sciences, Glasgow Caledonian University, City Campus, Cowcaddens Road, Glasgow, G4 OBA, Scotland.

Corresponding Author: Chris Bartholomew
email: c.bartholomew@gcu.ac.uk
Phone: 0141-331-3213

Acknowledgments:
We would like to thank the Dept. of Biological & Biomedical Sciences, GCU technical staff, Fiona Biggerstaff and Ann Marie Clark for continuous assistance throughout this project. In addition we would like to thank HONS project students Rebecca McPeak, Claire Wallace, Jonathon Willock and Rabia Ashraf for their contribution to this work. This work was supported by Glasgow Caledonian University and a PhD studentship (MAH) from the Kuwait Cultural Bureau, London, UK.

Abstract: Obesity-associated conditions represent major global health and financial burdens and understanding processes regulating adipogenesis could lead to novel intervention strategies. This study shows that adhesion G-protein coupled receptor 56 (*GPR*56) gene transcripts are reduced in abdominal visceral white adipose tissue derived from obese Zucker rats vs lean controls. Immunostaining in 3T3-L1 pre-adipocytes reveals both mitotic cell restricted surface and low level general expression patterns of Gpr56. *Gpr*56 transcripts are differentially expressed in 3T3-L1 cells during adipogenesis. Transient knockdown (KD) of *Gpr*56 in 3T3-L1 cells dramatically inhibits differentiation through reducing the accumulation of both neutral cellular lipids (56%) and production of established adipogenesis Pparγ_2 (60-80%), C/ebpα (40–78%) mediator and Ap2 (56-80%) marker proteins. Furthermore, genome editing of *Gpr*56 in 3T3-L1 cells created CW2.2.4 and RM4.2.5.5 clones (*Gpr*56$^{-/-}$ cells) with compound heterozygous deletion frameshift mutations which abolish adipogenesis. Genome edited cells have sustained levels of the adipogenesis inhibitor β-catenin, reduced proliferation, reduced adhesion, altered profiles and or abundance of extracellular matrix component gene transcripts for fibronectin, types I, III and IV Collagens and loss of actin stress fibres. β-catenin KD alone is insufficient to restore adipogenesis in *Gpr*56$^{-/-}$ cells. Together these data show that Gpr56 is required for adipogenesis in 3T3-L1 cells. This report is the first demonstration that Gpr56 participates in regulation of the adipogenesis developmental programme. Modulation of the levels of this protein and/or its biological activity may represent a novel target for development of therapeutic agents for the treatment of obesity.

Key Words: *GPR*56; Adipogenesis; Knockdown; Genome editing; β-CATENIN; Extracellular matrix.

Introduction: Obesity and associated diseases including type II diabetes, heart disease and cancer represent major global health and financial burdens and understanding the molecular basis of adipogenesis could identify novel therapeutic strategies for treatment. G-protein coupled receptors (GPCR's) are involved in the regulation of adipose tissue but in many cases their function has not been investigated. GPCR's comprise a large gene family of which adhesion G-protein coupled receptors represent a sub-group of 33 members in the human genome (Mehta & Piao, 2017). *GPR*56 (*ADGRG*1) is a member of this sub-group and the encoded protein is associated with brain cortical patterning. Well characterised mutations of *GPR*56 cause a rare autosomal recessive brain deformity, associated with severe mental retardation, motor and language impairment and epilepsy, called bilateral frontoparietal microgyria (Piao et al., 2004). *Gpr*56 null mice display a defect in adhesion of developing neurons (Koirala et al., 2009) and despite the apparent absence of further phenotypic defects in these animals, GPR56 has also been associated with other biological roles including pancreatic β-cell function (Duner et al., 2016), muscle hypertrophy (White et al., 2014), tumorigenesis (Aust et al., 2016) and maintenance of haemopoietic stem cells (Rao et al., 2015)(Saito et al., 2013).

*GPR*56 is expressed in adipocytes (Amisten et al., 2015) and several observations are consistent with a possible role in adipogenesis. Two ligands have been identified for GPR56, type III collagen [COL3A1] (Luo et al., 2011) and transglutaminase 2 [TGM2] (Xu et al., 2006). TGM2 is present in white adipose tissue and has been shown to inhibit adipogenesis in *Tgm*2 null mouse embryo fibroblasts (Myneni et al., 2015). The absence of Tgm2 correlates with reduced nuclear β-catenin, a negative regulator of adipogenesis (Ross et al., 2000), as well as reduced Rock kinase activity. COL3A1 stimulates RHOA when bound to GPR56 in neural progenitor cells via activation of the α subunits of heterotrimeric $G_{12/13}$ proteins (Iguchi et al., 2008). A role for a cryptic GPCR in adipogenesis is suggested by *Pasteurella multicida* toxin mediated activation of $G_{12/13}$ protein subunits resulting in suppression of 3T3-L1 cell differentiation (Bannai et al., 2012). Activation of $G_{12/13}$ protein subunits stimulate RHOA which in turn activates ROCK1 and ROCK2 kinases. Pharmacological inhibition of Rock2 kinase with Y27632 in 3T3-L1 cells mediates differentiation to adipocytes in the absence of the normal chemical cocktail required to execute this development programme (Papers & Doi, 2007). Thus, evidence suggests that stimulation of the $G_{12/13}$ α protein/RHOA/ROCK pathway inhibits adipogenesis. Therefore, modulation of adipogenesis

by the same proteins which mediate GPR56 signalling indicates a potential link with this developmental programme.

The fibroblast-like 3T3-L1 cell line is a valuable model system to study adipogenesis (Todaro & Green, 1963). Hormonal stimulation initiates differentiation into an adipocyte-like phenotype and induction of a cascade of transcription factors mediating adipogenesis including key regulator CAAT enhancer binding proteins (C/EBP) (Cao et al., 1991) and peroxisome proliferator activated receptor proteins (PPAR) (Tontonoz et al., 1994). C/EBPβ is rapidly and transiently induced and regulates the production of C/EBPα and PPARγ which in turn control expression of target genes required for adipogenesis. Enforced expression or depletion of C/EBPβ, inhibits and enhances adipogenesis respectively (Schroeder-Gloeckler et al., 2007). PPARγ is essential to execute this developmental programme (Rosen et al., 2002).

The current study characterises the expression of *GPR*56 in adipose tissue from lean and obese rats and 3T3-L1 cells and investigates the role of GPR56 in adipogenesis by knockdown and genome editing in these cells.

Materials and Methods

Animal studies All studies were approved by the Institute's Animal Welfare and Ethical Review body and carried out in accordance with the UK Animals Scientific Procedures Act (1986).

Zucker Rats Abdominal visceral white adipose tissue was collected from obese Zucker male rats (*fa*/*fa*; n=6) and lean male littermates (*fa*/-; n=6), purchased from Harlan laboratories (UK). Animals were aged 17-20 wks with mean weights of 374.2g, SEM 51.8g (Lean) and 559.5g, SEM 27.6g (Obese). Animals were euthanized by intraperitoneal administration of pentobarbital (5mg/100g) [pharmasol, JM Loveridge PLC, Southampton, UK] and tissues collected and immediately stored at -80C.

Preparation of Total Cellular RNA, cDNA Synthesis and Quantitative Real-time Polymerase Chain Reaction RNA was prepared from cultures of cells by the TRI Reagent® method (Sigma-Aldrich, 93289). RNA from adipose tissue was prepared by first homogenizing 50mg of sample in 1ml TRI Reagent with 50µl 0.1mm glass beads (Biospec products Inc, Bartlesville, Oklahoma, U.S.A.) using a FASTPREP FP120 (Thermo Electron Corporation, Beverly, Massachusetts, U.S.A.). One µg of total cellular RNA was used to synthesise cDNA using SuperScript III First-Strand Synthesis SuperMix cDNA synthesis kit (Invitrogen, 18080) according to the manufacturer's instructions. 1.5 % of the cDNA reaction was used for quantitative real-time polymerase chain reaction using SYBR Green Rox mix (Thermo Fisher Scientific, Waltham, Massachusetts, U.S.A., 11873913), gene specific oligonucleotide primers, 95°C, 15mins followed by 40 cycles 95°C, 15s, 60°C, 60s in a CFX96 C1000 Thermal cycler (BIO-RAD Laboratories Ltd., Hemel Hempstead, UK). Relative expression levels between target and calibrator genes were determined using the arithmetic comparative $2^{-\Delta\Delta Ct}$ method (Livak & Schmittgen, 2001).

Cell Culture 3T3-L1 (ATCC®CL-173™) cells were cultured in complete medium (CM) comprising Dulbecco's Modified Eagle's Medium (Lonza Group Ltd, Basel, Switzerland, BE12-604F) supplemented with 10% v/v newborn calf serum (3T3-L1) (Sigma-Aldrich, Poole, UK, N4637) and 2.5mM glutamine, 50units/ml penicillin, 50µg/ml streptomycin (Lonza Group Ltd, BE17-605E & BE17-603E), 37°C, 5% CO_2. For differentiation, 3T3-L1 were maintained at 100% confluence for 48hrs prior to supplementing with induction medium 1 (IM1), comprising CM with 10% v/v foetal calf serum (Lonza, DE14-801F), 5µg/ml insulin (Sigma-Aldrich, I9278), 0.25µM dexamethasone (Sigma-Aldrich, D4902), 0.5mM Isobutylmethylxanthine (IBMX, Sigma-Aldrich I5879) for 48hrs, followed by

incubation with induction medium 2 (IM2) comprising CM supplemented with 10% FCS and 5μg/ml insulin every 48hrs up to 10 days. siRNA transfected cells were induced to differentiate as above 72hrs post-transfection. For genome editing, semi-confluent cultures of 3T3-L1 cells were transfected with 1μg each recombinant gRNA, hCas9 (gift from George Church, Addgene plasmid # 41824 and 41815 (Mali et al., 2013)) and pC1 (recombinant pSIREN-RetroQ vector [Clontech, Mountain View, California, USA, 631526] with scrambled control shRNA inserted (*Bartholomew, unpublished*)) plasmid DNA's using Lipofectamine 3000 (ThermoFisher Scientific Inc., St. Leon-Rot, Germany, L300000) according to manufacturer, 48hrs, then CM supplemented with 2μg/ml puromycin (Sigma-Aldrich, P8833) 96hrs. Single cell clones were derived from isolated colonies. Media was removed from cells which were then rinsed with Phosphate buffered saline (PBS, Lonza, BE17-516F), overlayed with trypsin-EDTA (Lonza BE17-161E) saturated sterile filter paper discs (Whatmann 1MM, Fisher Scientific, Loughborough, UK), incubated for 5mins, 37ºC and discs plus cells transferred to 24 well culture dish with 500μl CM. Cell numbers were determined using a haemocytometer counting chamber (Neubauer Marienfeld, Paul Marienfeld GmbH & Co. KG, Germany) and inverted microscope (CK2, Olympus UK Ltd, Southend-on Sea, UK).

Immunostaining Cells were cultured on sterile 16mm^2 microscope coverslips, washed with ice cold PBS and fixed with ice cold 4% w/v paraformaldehyde for 10mins at room temperature (rt). Permeabilised cells were treated with 0.1% (v/v) Triton™ X-100 (Sigma-Aldrich, T8787) in PBS, 10 min, rt then washed in PBS 15min, rt. Both permeabilised and non-permeabilised cells were incubated 60mins, rt in blocking buffer (PBS, 0.2M glycine, 10% v/v FCS) then o/n, 4°C, with primary antibody α-GPR56 (Merck KGaA, Darmstadt, Germany, H11) or α-VSVG (Santa Cruz Biotechnology Inc, Santa Cruz, CA, U.S.A., F-6). Cells were washed 40mins at rt in PBS and incubated for 1.5hr at rt with secondary antibody Goat α-mouse IgG H&L Alexa Fluor® 488, (abcam ab150113) in blocking buffer. Cells were washed in PBS for 1hr at rt, counterstained with DAPI-hydrochloride (ThermoFisher, D1306) for 1min at rt and washed in PBS for 1min at rt and then mounted with Fluorosave™ (Millipore 345789). Alternatively, fixed, permeabilised cells were incubated with 165nM Alexa Flour™ 488 Phalloidin (A12379, Invitrogen) in PBS, 1hr at rt and washed and stained with DAPI as above. Image acquisition was performed using a LSM 800 confocal microscope with a 63Å~/1.4 NA oil immersion objective using ZEN 2.3 (blue edition) software (Carl Zeiss GmbH, Jena, Germany).

Oil Red O Staining and Quantitation Cells were washed in ice cold PBS, fixed in 10% v/v formaldehyde for 10 minutes at room temperature (rt) and incubated sequentially in 60% isopropanol for 1 hour at rt in 6% w/v Oil Red O (Sigma-Aldrich, O0625, in 60% isopropanol), then ice cold PBS. For quantitation, Oil Red O stain was extracted with 50% culture volume of 100% isopropanol for 5minutes and absorbance read at 492nm using an Epoch plate reader (Biotek Instruments Inc, Plainfield, NJ, USA).

Oligonucleotide Primers Oligonucleotide primers were synthesised by Integrated DNA Technologies (IDT, BVBA, Leuven, Belgium) (see table below for sequences).

Gpr56F: CCGAGCTTCATCTTCTCCTTC	Gpr56R: GCTGCTGCAATTCCTTCTTG
18SF: ACCGCAGCTAGGAATAATGGA	18SR: GCTTCAGTTCCGAAAACCA
ratgpr56F: CTAACCTCTCAGATCCCGTGGTA	ratgpr56R: CACACTGCAGAGTCACGTTCTTT
gapdhF: CTGACATGCCGCCTGGAGAAA	gapdhR: CCACCCTGTTGCTG TAGCCAT
Pparγ_2F: GCCCACCAATTCCGGCAATC	Pparγ_2R: TGCGAGTGGTCTTCCATCAC
C/ebpαF: GAGCTGAGTGAGGCTCTCATT	C/ebpαP: TGGGAGGCAGACGAAAAAAC
Ap2F: GGGCATGGAATTCGATGAAATCA	Ap2R: CCCGCCATCTAGGGTTATGAT
β-cateninF: ACTAAGCAGGAAGGGATGGA	β-cateninR: ATGACGAAGAGCACAGATGG
JWgF: TTTCTTGGCTTTATATATCTTGTGGAAA GGACGAAACACCGGATAGAGCCCTCTAGGCTC	JWgR:GACTAGCCTTATTTTAACTTGCTATTT CTAGCTCTAAAACGAGCCTAGAGGGCTCTA TC
RMgF: TTTCTTGGCTTTATATATCTTGTGGAAA GGACGAAACACCGGGAGACTCCACTTGCGCTA	RMgR:GACTAGCCTTATTTTAACTTGCTATTT CTAGCTCTAAAACTAGCGCAAGTGGAGTCTC C
Alt-RF: GAGAAGACTTCCGCTTCTGTG	Alt-RR CTCCATCCCTTGTTCTCTGTG
RAF: GCTCTATCACTTCTGCCTCTAC	RAR: AATCTGCCAGGAGCTGAC
JWF: CAGAGGAGACCCTCACAATTC	JWR: CTTGGCTACTAAGCAGGTAGTC
Fn1F: TACGGAGAGACAGGAGGAAATA	Fn1R: CATACAGGGTGATGGTGTAGTC
Col1α1F: AGACCTGTGTGTTCCCTACT	Col1α1R: GAATCCATCGGTCATGCTCTC
Col3α1F: CTGTAACATGGAAACTGGGGAAA	Col3α1R: CCATAGCTGAACTGAAAACCA CC
Col4α1F: GGTCCTGTCTGGAAGAGTTTAG	Col4α14R: TGAACATCTCGCTTCTCTCTATG
Col6α1F: TGCCCTGTGGATCTATTCTTCG	Col6α1R: CTGTCTCTCAGGTTGTCAATG
LKO.1: GACTATCATATGCTTACCGT	

siRNA-Mediated Gene Knockdown 2X10^4 3T3-L1 cells were seeded in a 24-well plate, cultured for 24hrs then transfected with *Gpr*56 30nM Dicer-Substrate siRNAs, G-DsiRNA 1, 2, 3 or S. DsiRNA (IDT, #157187617, #157187609, #157187606, #51-01-19-09) or β-catenin Dicer-Substrate siRNAs BcatsiRNA's 1, 2 and 3 (IDT, #76963822, #7696819, #76963816) , using Lipofectamine™ RNAiMAX for 48hrs according to the manufacturer's instructions (Invitrogen, 13778030).

Western Blot Analysis Cultured cells were mechanically harvested in ice-cold RIPA buffer (1% NP-40, 50mM TrispH7.6, 120mM NaCl, 1mM EDTA) containing protease inhibitor cocktail (P8340) and phosphatase inhibitor cocktail 3 (P0044) (Sigma-Aldrich), incubated on ice for 30mins then centrifuged 13,000rpm, 20mins at 4°C. Protein concentration was

196 determined using the Bicinchoninic acid protein assay method (Stoscheck, 1990). Equal
197 quantities of proteins were separated by SDS-polyacrylamide gel electrophoresis and
198 transferred to nitrocellulose. Nitrocellulose bound total protein was used for quantification
199 using the REVERT™ total protein stain kit according to the manufacturer's instructions
200 (926-1101, LI-COR™, Lincoln, Nebraska, U.S.A.) and analysed at 700nm using an Odyssey
201 FC image analyser (LI-COR®). Subsequently, membranes were washed in REVERT™
202 reversal solution and western blotting performed with antibodies to α-GPR56 (Merck, H11),
203 α-PPARγ (C26H12), α-C/EBP-α (2295), α-βACTIN (8H10D10), Total β-catenin (D10A8),
204 Active β-catenin (D13A1) (Cell Signaling Technologies ®, Leiden, The Netherlands), or α-
205 AP-2 (Santa Cruz Biotechnology Inc, C-15) at 1:1000 dilution. Appropriate IRDye®800CW
206 conjugated α-goat (926-32214), IRDye®800CW conjugated α-rabbit (926-32211) or IRDye®
207 680RD conjugated α-mouse (926-68072) (LI-COR®) IgG secondary antibodies were used at
208 1/15000 dilutions. Detection was performed by fluorescence using an Odyssey FC image
209 analyser (LI-COR®) and analysed with Image Studio Software Lite Ver 5.2 (LI-COR®).
210 ***Creation of Retroviral and gRNA Vectors and Preparation of Plasmid DNA***
211 Guide RNA (gRNA) plasmid vectors pCW2 and pRM4 were created using the gRNA cloning
212 vector (gift from George Church Addgene ID 41824) (Mali et al., 2013). CRISPR targets in
213 murine *Gpr*56 exon 3 sequence (Adgrg1-202, ENSMUST00000179619.8) were identified
214 using a CRISPR design tool (http://crispr.mit.edu). Two target sequences were selected and
215 oligonucleotides CWgF, CWgR RMgF and RMgR synthesized. Primer annealing and
216 extension was performed with 0.5μM each of either CWF and CWR or RMF and RMR in 1X
217 5XPhusion® HF buffer, 200μM dNTP's, 1 unit Phusion® DNA polymerase (New England
218 Biolabs, M0530) in 50μl, 98°C 30sec, 40 cycles of 98°C 10sec, 52°C 30sec, 72°C 30sec
219 followed by 72°C 2mins in a MJ Scientific programmable thermocycler. Annealed DNA was
220 gel-purified (Nucleospin® Gel and PCR clean-up). *Bsp*TI (ThermoFisher Inc., ER0831)
221 linearised gRNA cloning vector and annealed DNA fragments were combined with Gibson
222 assembly master mix (New England Biolabs, E5510) in 10μl and incubated 50°C, 1h and 2μl
223 used to transform NEB 5-alpha high efficiency competent cells (New England Biolabs,
224 E5510). All plasmid DNA was prepared by affinity chromatography using Nucleobond®
225 PC500EF gravity flow columns according to manufacturer's instruction (Macherey-Nagal
226 GmbH). pCW2 and pRM4 gRNA target sequence was confirmed using LKO.1 primers.
227 ***Isolation of Genomic DNA and Heteroduplex Analysis*** DNA was isolated from 10,000-
228 15,000 cells in 96 well culture dish using 50μl QuickExtract DNA isolation solution

(Lucigen, Cambridge, UK, QE09050), vortexed 30sec, incubated 65ºC 10 mins, 98ºC 5 mins and diluted in 100µl nuclease free water. DNA was amplified with 40ng genomic DNA, 300nM Alt-RF and Alt-RR primers, 1X DreamTaq Green PCR master mix (ThermoScientific, K1081) in 25µl, 95ºC 90sec, 40 cycles 95ºC 30sec, 65ºC 30secs, 72ºC 30 sec and 72ºC 5mins using a MJ Scientific programmable thermocycler. Amplified DNA (20%), 1X T7EI reaction buffer (Alt-R Genome Editing Detection Kit, Integrated DNA Technologies, 1075932) in 10µl was denatured 95ºC 10mins, annealed 95-85ºC (Ramp rate -2ºC/sec), 85-25ºC (Ramp rate -0.3ºC/sec) and digested 1U T7 DNA endonuclease 1 hour 37ºC in a MJ Scientific programmable thermocycler.

Identification of Mutant Alleles Genomic DNA was amplified by PCR with either RAF/RAR (RM cells) or JWF/JWR (CW cells) primers with DreamTaq as described above. Amplified DNA was inserted into pJET1.2 cloning vector using CloneJET PCR cloning kit (ThermoScientific, K1231) according to manufacturer's instructions and used to transform DH5-α competent cells (Invitrogen, 18265-017). Individual colonies were picked for colony PCR with pJET1.2 Forward and Reverse primers (ThermoScientific, K1231) with DreamTaq**.** Amplified DNA was sequenced using the pJET1.2 Forward primer.

Sequencing Sequences were determined by Sanger sequencing of plasmid and PCR amplified DNA using the automated LIGHTRUN™ DNA sequencing service (Eurofins Genomics, Constance, DE). DNA sequence analysis was performed using SnapGene DNA viewer 3.3.4.

Cell Proliferation assay The AlamarBlue® cell proliferation assay (DAL1025, Invitrogen™) was used according to manufacturer's instructions. $5X10^2$ cells/well were seeded in 96 well plates in CM and refed every 24hrs. Metabolic activity was determined every 24hr in CM supplemented with 10% AlamarBlue® for 4hr. AlamarBlue® reduction was determined from absorbance at 570nm and 600nm using a FLUOstar® Omega plate reader (BMG LABTECH LTD).

Cell Adhesion Assay One thousand cells/well were seeded in CM and incubated in 96 well plates for 6hr, 37°C, 5% CO_2. Medium was removed, cells washed in PBS, fixed with 10% (v/v) formaldehyde in PBS 10min rt, rinsed 2X with PBS then stained with 0.1% (w/v) crystal violet (CO775, Sigma- Aldrich) in 2% ethanol 10 min, rt. Cells were washed in PBS, crystal violet extracted in 2% SDS then absorbance 570nm determined with an Epoch plate reader.

Statistical Analysis Data are expressed as the mean ± standard error of the mean from at least 3 independent experiments. Statistical significance was determined by one-way ANOVA, two-way ANOVA, unpaired two-tailed Student t-test or multiple t-test as indicated, using GraphPad PRISM® 7.0c software. $P \leq 0.05$ was considered significant.

Results

GPR56 is Differentially Expressed in Adipose Tissue and 3T3-L1 cells

The abundance of *GPR*56 gene transcripts was compared in abdominal visceral white adipose tissue from lean vs obese Zucker rats by reverse-transcription quantitative real-time polymerase chain reaction (QPCR) with oligonucleotide primers specific for rat *gpr*56 (ratgpr56F&R) as described in Materials and Methods. Levels of *gpr*56 gene transcripts were significantly lower in white adipose tissue from obese (50-60% reduction) vs lean rats (Fig.1A).

We next examined Gpr56 expression in 3T3-L1 preadipocytes. Immunostaining with α-Gpr56 showed a low level of either general staining (Fig.1B, + permeabilised) in all cells or punctate cell surface staining that is observed in mitotic cells only (Fig.1B, - non-permeabilised). Next *Gpr*56 gene expression was investigated at various stages of the adipogenesis differentiation programme. Cultures of 3T3-L1 cells were induced to differentiate and at various time points either stained with Oil Red O or total cellular RNA isolated for QPCR (Materials and Methods). An increased accumulation of Oil-red O stained neutral lipids (Fig.1C) and gene transcripts of regulators and markers (*C/ebpα*, *Pparγ*$_2$, adipocyte factor 2 *Ap*2, *data not shown*) was observed in 3T3-L1 cells as differentiation progressed confirming execution of the adipocyte developmental program. QPCR results confirmed *Gpr*56 gene transcripts in 3T3-L1 cells (Fig.1D). Expression levels vary moderately with an initial decline followed by an increase reaching maximum levels 6 day's post-induction (Fig.1D).

Gpr56 Knockdown Inhibits 3T3-L1 Cell Adipocyte Differentiation The impact of loss of endogenous Gpr56 on 3T3-L1 differentiation was investigated by gene knockdown (KD) using Dicer-Substrate Short Interfering RNAs (DsiRNA's). *Gpr*56 KD efficiency of three DsiRNAs, targeting exons 3, 11 or 14 (Fig.2A) were tested. All three KD 3T3-L1 *Gpr*56 gene transcripts (S1A) and the most effective, G-DsiRNA 2 (90% KD), was selected for further analysis.

Initially KD of *Gpr*56 transcripts was examined in 3T3-L1 cells through differentiation for up to 10 days. *Gpr*56 transcripts initially decline between 0 and 2 days with control S- siRNA (scrambled) and then are induced in days 3, 4, 6 and 10 (Fig.2B) in a similar manner to untreated 3T3-L1 cells (Fig.1D). However, G-DsiRNA 2 treated 3T3-L1 cells show decreased *Gpr*56 transcripts in both pre-adipocytes and through the differentiation program

299 although again expression increases from day 3 to 10 (Fig.2B, S siRNA vs G-DsiRNA 2).
300 Cells are transfected once with DsiRNA's (Materials and Methods) and therefore the late
301 increase in transcripts show inhibition of *Gpr*56 expression is only transient. 3T3-L1 cells
302 were also immunostained with α-Gpr56 24hrs post-transfection with either control S- siRNA
303 or G-DsiRNA 2 (Fig.2C). The results show a significant reduction of general staining in G-
304 DsiRNA 2 vs S-siRNA treated cells (66%, S1B), confirming a reduction in Gpr56 protein in
305 KD cells.
306 G-DsiRNA 2 treatment dramatically inhibits 3T3-L1 cell adipogenesis, significantly reducing
307 the accumulation of neutral lipid staining with Oil-red O at both days 4 and 10 by 64% and
308 56% respectively (Fig.3A, S1C). In contrast control, scrambled DsiRNA had no effect on
309 3T3-L1 cell neutral lipid accumulation (Fig.3A, S1C). Inhibition of 3T3-L1 cell
310 differentiation was also observed with the alternative G-DsiRNA 1 (S2). Western blot
311 analysis showed Pparγ_2, C/ebpα and Ap2 proteins are induced during differentiation of both
312 scrambled S. siRNA and DsiRNA 2 transfected 3T3-L1 cells (Fig.3B) but quantitative
313 analysis reveals a significantly reduced accumulation in DsiRNA 2 treated cells at days 4
314 (Pparγ_2-80%, C/ebpα−78%, Ap2-80%) and 10 (Pparγ_2-60%, C/ebpα−40%, Ap2-56%)
315 (Fig.3B, S1C). QPCR analysis also shows a significant reduction in *Ppar*γ_2 (35%-50%) and
316 *Ap*2 (23%-70%) gene transcripts at days 4, 6 and 10 in G-DsiRNA 2 vs control S. siRNA
317 treated cells (S3), consistent with western blot analysis. Sustained active β-catenin inhibits
318 adipogenesis (Ross et al., 2000) and this was also investigated by Western blot analysis.
319 Results show a reduction in active β-catenin at day 4 (48%) and 10 (72%) relative to day 0 in
320 control S. siRNA differentiating 3T3-L1 cells whereas levels are initially higher (168%, day
321 0 G-DsiRNA 2 vs S. siRNA treated 3T3-L1 cells) and decline only moderately throughout
322 differentiation of DsiRNA 2 treated cells (Fig. 3B, S1D).
323
324 *Inhibition of Adipogenesis in Gpr56 Genome Edited 3T3-L1 cells* To investigate the role of
325 Gpr56 further, genome edited 3T3-L1 cell lines were created with targeted *Gpr*56 gene
326 mutations. Two sites within the Gpr56 gene were selected for genome editing and guide RNA
327 (gRNA) plasmid vectors pCW2 and pRM4, which target sequences within exon 3 as shown
328 in Fig.2A, were created (Materials & Methods). 3T3-L1 cells were transfected with gRNA,
329 pCAS9 and pC1 plasmid DNA's, transiently selected with puromycin and single cell cloned
330 as described in Materials and Methods. Single cell clones were screened for the presence of
331 INDELS in the *Gpr*56 gene by heteroduplex analysis (S4 A). A DNA cloning and sequencing

strategy was adopted to screen cell clones for INDEL frameshift mutations (Materials and Methods). A total of 17 pCW2 (CW cells) and 21 pRM4 (RM cells) derived single cell clones with INDELS were sequenced and 3 clones with compound heterozygous deletion frameshift mutant *Gpr*56 alleles identified. The partial sequences of the mutant alleles in clones CW2.2.4 and RM4.2.5.5, which were chosen for further study, are shown in Figure 4. Immunostaining with α-Gpr56 in CW2.2.4 and RM4.2.5.5 cells revealed both significantly reduced staining (75%-84 %) as well as a change in cellular localisation compared to parental 3T3-L1 cells (S4 B, C), confirming loss of expression.

Adipogenesis in genome edited cells was determined by Oil Red O staining (Materials and Methods). CW2.2.4, RM4.2.5.5 and 3T3-L1 cells were induced to differentiate (Materials and Methods) and cells stained at days 0, 4 and 10. The results show the expected accumulation of Oil Red O stained neutral cellular lipids in 3T3-L1 cells at days 4 and 10 but a dramatic and highly significant reduction in staining of both genome edited cell lines (76-77% day 4 and 87-88% day 10) (Fig.5A, S5 A). Furthermore, Western blot analysis showed no significant induction of Pparγ_2, C/ebpα and Ap2 proteins in RM4.2.5.5 cells (Fig.5B, S5 B), which is consistent with Oil red O staining data. Western blotting again showed sustained active β-catenin in differentiating genome edited cells (Fig.5B, S5 B). β-catenin KD was used to see if adipogenesis could be restored in RM4.2.5.5. BcatsiRNA 3 was chosen from three DsiRNA's tested as it significantly reduced total β-catenin protein (92%) in 3T3-L1 cells (S6 A, B, C) but treatment of RM4.2.5.5 cells failed to restore adipogenesis (S6 D).

Gpr56 genome edited cells show reduced proliferation, adhesion, actin stress fibres and altered extracellular matrix gene expression Gpr56 is associated with cell proliferation and adhesion and these properties were examined to further investigate the impact of Gpr56 loss in 3T3-L1 cells. Results show that both RM4.2.5.5 and CW2.2.4 cell lines have significantly reduced proliferation rates vs 3T3-L1 cells (Fig.6A). Furthermore, both cell lines show significantly reduced adhesion compared with parental cells (Fig.6B). Gene transcripts encoding extracellular matrix (ECM) proteins fibronectin (*Fn*1) and types 1 (*Col*1α1), III (*Col*IIIα1) IV (*Col*4α1), VI (*Col*6α1) collagens were compared by QPCR (Materials and Methods) in preadipocytes (day 0) and at 10 days post differentiation in 3T3-L1 vs RM4.2.5.5 cells. The results show significant differences for *Fn*1, *Col*1α1 and *Col*4α1 gene transcripts in the presence (3T3-L1) and absence of Gpr56 (RM4.2.5.5). Normally, *Fn*1 and *Col*1α1 gene transcripts decline and *Col*4α1 and *Col*6α1 transcripts increase as 3T3-L1 cells

differentiate (Fig.6C). However, *Fn*1 is significantly decreased in preadipocytes (74% reduction in RM4.2.5.5 vs 3T3-L1) and induced 4 fold at 10 days in RM4.2.5.5 relative to 3T3-L1. *Col*1α1 transcripts are significantly elevated in preadipocyte RM4.2.5.5 cells (>2 fold in 3T3-L1 vs RM4.2.5.5) and decline to 3T3-L1 cell levels at day 10. *Col*4α1 transcripts are similar in both preadipocyte cells but significantly less at 10 days differentiation in RM4.2.5.5 vs 3T3-L1 (reduced 74%). The level of *Col*3α1 are slightly increased in RM4.2.5.5 relative to 3T3-L1 cells but decline in both cases during differentiation. The levels and induction of *Col*6α1 during differentiation are the same in both cell types (Fig.6C).

Significant changes in the organization of the actin cytoskeleton occur during differentiation of adipocytes (Nobusue et al., 2014). To examine actin cytoskeleton, 3T3-L1 and RM4.2.5.5 preadipocytes were stained with fluorescently labelled Phalloidin (Materials and Methods). The results show a significant difference in F-actin organization (Fig.7A) and quantity (Fig.7B) in RM4.2.5.5 vs 3T3-L1 cells. 3T3-L1 cells show F-actin organized in stress fibres whereas RM4.2.5.5 cells show reduced, thin stress fibres, staining of the cell cortex (Fig.7A) and generally reduced staining intensity (Fig.7B, 25% reduction).

Discussion

Several GPCR's regulate adipogenesis (Eisenstein, 2013) and GPR56 expression has been observed in adipocytes previously (Amisten et al., 2015). In this study, we show for the first time that GPR56 is necessary for adipogenesis *in vitro*. Data generated from our *in vitro* studies show both KD and genome editing of GPR56 is inhibitory. The finding that levels of *gpr*56 transcripts are lower in adipose tissue from genetically obese rats supports the hypothesis that dysregulation of expression of this receptor may be linked to adipocyte hypertrophy or hyperplasia. The impact of complete loss of Gpr56 on adipogenesis *in vivo* is unknown but knockout mice fed a high fat diet have a metabolic phenotype, but similar weight gain, compared to wild type animals (Spaethling et al., 2016). Further studies are required to investigate the expression of *Gpr*56 in fat depots in these and other genetic and diet induced animal models of obesity to extend the observations made here.

Our results show that low levels of endogenous Gpr56 protein are seen in 3T3-L1 preadipocytes. Confocal analysis shows a general staining of cells, not seen with either isotype control or secondary antibody control antibodies, in permeabilised cells. The reduction in staining observed with both Gpr56 KD and genome edited cells confirms this is Gpr56. It is not clear why residual staining is still observed in the Gpr56 genome edited ($Gpr56^{-/-}$) cells, but it could be due to production of a truncated protein that retains the epitope recognized by the antibody used for this study.

Low levels of cell surface Gpr56 are also detected in immunostained non-permeabilised 3T3-L1 preadipocytes. Interestingly, we only detect cell surface staining in mitotic cells, suggesting its localization might be regulated during cell division and/or contribute to this process. The significance of this M-phase specific staining requires further investigation but is consistent with other studies that suggest GPR56 participates in cell proliferation (Ackerman et al., 2015)(Bae et al., 2014).

Both KD and $Gpr56^{-/-}$ cells show that loss of Gpr56 reduces or abolishes adipogenesis in 3T3-L1 cells as demonstrated by reduced accumulation of: 1) neutral cellular lipids; 2) developmental marker protein Ap2 and 3) key regulators of adipocyte differentiation, Pparγ_2 and C/ebpα. The $Gpr56^{-/-}$ cell phenotype is more severe than the KD phenotype. KD results in only a transient reduction in *Gpr*56 in preadipocytes at the early stages of differentiation, as transcripts recover at later stages of the developmental programme (Fig.2B days 6 and 10). This suggests Gpr56 is important at early stages of the process. The partial differentiation observed in KD cells could be due to either insufficient reduction of Gpr56 or an overall delay to the process which can still occur as levels recover. Alternatively Gpr56

might be required for both early and late events in adipogenesis which could also explain the complete abrogation of differentiation observed in *Gpr*56$^{-/-}$ cells. This possibility is consistent with the biphasic expression pattern observed for *Gpr*56 transcripts from preadipocytes through to adipocytes. In the current study 3T3-L1 cells were found to express low levels of endogenous *Gpr*56 gene transcripts which consistently vary during differentiation with an initial decrease followed by a subsequent increase that plateaus at 6 to 10 days (Fig.1D, Fig.2B). It is unclear if the biphasic change in *Gpr*56 transcripts is required for differentiation as it is unknown if this coincides with changes in protein production.

The data presented suggest Gpr56 modulates adipogenesis through changes in the production of known regulators of this process. PPARγ is a master regulator of adipogenesis and can initiate the entire differentiation program (Farmer, 2006) even in the absence of another key regulator of this developmental pathway, C/EBPα (Rosen et al., 2002). Levels of Pparγ$_2$ and C/ebpα are both reduced with decrease or loss of Gpr56 and therefore are most likely to be responsible for the inhibition of differentiation observed. The decreases in Pparγ$_2$ and C/ebpα are greater in *Gpr*56$^{-/-}$ cells vs KD cells which correlates with severity of suppression of adipogenesis.

A potential model for the impact of Gpr56 loss on adipogenesis is shown in figure 8. The mechanism of inhibition is unknown but could involve changes to one or more of:- 1) β-catenin; 2) cell proliferation; 3) cell adhesion; 4) ECM and 5) actin cytoskeleton. Numerous studies show that changes to any of these properties affect adipogenesis. Active β-catenin is a known inhibitor of adipogenesis and Pparγ$_2$ gene expression (Okamura et al., 2009) and studies suggest a link between Gpr56 and β-catenin activity (Shashidhar et al., 2005). However, β-catenin KD alone is insufficient to restore adipogenesis in *Gpr*56$^{-/-}$ cells suggesting other inhibitory mechanisms also contribute. Stimulation of cell proliferation inhibits adipogenesis (Hu et al., 1996) (Heath et al., 2000) (Abbott & Holt, 1997). GPR56 stimulates proliferation in various cell types including oligodendrocyte precursor (Ackerman et al., 2015), cortical progenitor (Bae et al., 2014) and fibroblasts (Ke et al., 2007) cells. Here we show loss of Gpr56 decreases 3T3-L1 cell proliferation. Reduced cell adhesion inhibits adipogenesis (Gabrielli et al., 2018)(Luo et al., 2008)(Kamiya et al., 2002) and GPR56 is a member of the adhesion GPCR family that is involved in adhesion of various cell types including developing neurons, haemopoietic stem cells and tumor cells (Shashidhar et al., 2005) (Koirala et al., 2009) (Yusuke et al., 2015). Here we show loss of Gpr56 reduces cell adhesion. Bioinformatics show cell ECM is one of the pathways commonly dysregulated in

453 both human and mouse obese adipose tissue (Berger et al., 2015). Changes to ECM
454 components including increased fibronectin or inhibition of collagen synthesis suppresses
455 adipogenesis (Kamiya et al., 2002)(Liu et al., 2017). GPR56 expression is associated with
456 changes in deposition of the ECM glycoprotein fibronectin (Millar et al., 2018). Here we
457 show elevated *Fn*1, *Col*1α1, *Col*3α1 and *Col*4α1 gene transcripts are all observed in *Gpr*56$^{-/-}$
458 cells suggesting changes to ECM composition. The coordinated disruption of actin stress
459 fibres is a prerequisite for adipogenesis (Nobusue et al., 2014). Enforced expression of
460 GPR56 induces Rho-dependent actin stress fibres in NIH3T3 cells (Iguchi et al., 2008). Here
461 we show *Gpr*56$^{-/-}$ cells already have significantly reduced actin stress fibres prior to
462 stimulation with differentiation signals.
463 Our results show that the consequences of loss of Gpr56 directly or indirectly changes several
464 properties that are all likely to contribute to inhibition of 3T3-L1 cell adipogenesis
465 (summarised in Fig. 8). The normal role of GPR56 in regulating adipogenesis is unclear from
466 these studies but we hypothesise that it may be related to its well characterised roles in cell
467 adhesion and actin stress fibre formation (Shashidhar et al., 2005)(Koirala et al.,
468 2009)(Yusuke et al., 2015)(Iguchi et al., 2008). It is well established that morphological
469 changes from fibroblast like to rounded cells occur in differentiation of adipocytes (Smas &
470 Sul, 2005) and this depends on both a reduction in cell adhesion and actin cytoskeleton
471 reorganization. Premature actin cytoskeleton reorganization inhibits adipogenesis but if
472 coordinated with standard differentiation signals, enhances the process (Titushkin et al.,
473 2013). Our results suggest GPR56 is necessary for the formation of actin stress fibres in
474 preadipocytes as they are dramatically reduced in Gpr56$^{-/-}$ cells. When preadipocytes are
475 stimulated to differentiate Gpr56 expression declines which could result in the reduction of
476 actin stress fibres allowing actin cytoskeleton reorganisation to occur enabling differentiation
477 to proceed. This model suggests that Gpr56 regulates early stages of differentiation,
478 consistent with the KD studies. Our results also show that Gpr56 levels recover after an
479 initial decline in the adipocyte developmental programme. This suggests Gpr56 may also
480 have a role at later stages of differentiation as well. Further studies are required to investigate
481 this possibility.
482 Stable enforced expression of Gpr56 enhances proliferation and adhesion and moderately
483 suppresses adipogenesis, causing reduced levels of Pparγ_2, C/ebpα, Ap2 and Oil red O
484 staining (*Hasan and Bartholomew, unpublished*). The reduced adipogenesis associated with
485 increased Gpr56 expression *in vitro* correlates with the inverse relationship seen with *gpr*56

expression in adipose tissue and weight gain *in vivo* in lean vs obese Zucker rats . It is possible that changes to the same cell properties described for $Gpr56^{-/-}$ cells also contribute to suppression of adipogenesis observed with enforced expression although the effect is less severe. The observation that both increased and decreased Gpr56 expression reduce adipogenesis in 3T3-L1 cells suggests that both agonists and antagonists of this G-protein coupled receptor could affect the development of adipocytes.

In summary, this investigation shows that *GPR*56 transcripts are reduced in adipose tissue of obese rodents and *in vitro* studies show that both enforced expression and loss of expression in 3T3-L1 cells suppress adipogenesis. Loss of Gpr56 has the greatest effect on the adipogenic developmental program. These studies suggest modulation of this protein and/or its biological activity could represent a target for development of novel therapeutic strategies for intervention in the treatment of obesity.

References

Abbott, D. W., & Holt, J. T. (1997). Finkel-Biskis-Reilly osteosarcoma virus v-Fos inhibits adipogenesis and both the activity and expression of CCAAT/enhancer binding protein α, a key regulator of adipocyte differentiation. *Journal of Biological Chemistry*, *272*(51), 32454–32462. https://doi.org/10.1074/jbc.272.51.32454

Ackerman, S. D., Garcia, C., Piao, X., Gutmann, D. H., & Monk, K. R. (2015). The adhesion GPCR Gpr56 regulates oligodendrocyte development via interactions with Gα12/13 and RhoA. *Nature Communications*, *6*(May 2014), 6122. https://doi.org/10.1038/ncomms7122

Amisten, S., Neville, M., Hawkes, R., Persaud, S. J., Karpe, F., & Salehi, A. (2015). An atlas of G-protein coupled receptor expression and function in human subcutaneous adipose tissue. *Pharmacology & Therapeutics*, *146*, 61–93. https://doi.org/10.1016/j.pharmthera.2014.09.007

Aust, G., Zhu, D., Van Meir, E. G., & Xu, L. (2016). Adhesion GPCRs in Tumorigenesis. *Handbook of Experimental Pharmacology*, *234*, 369–396. https://doi.org/10.1007/978-3-319-41523-9_17

Bae, B.-I., Tietjen, I., Atabay, K. D., Evrony, G. D., Johnson, M. B., Asare, E., … Walsh, C. A. (2014). Evolutionarily Dynamic Alternative Splicing of GPR56 Regulates Regional Cerebral Cortical Patterning. *Science*, *343*(6172), 764 LP – 768. http://science.sciencemag.org/content/343/6172/764.abstract

Bannai, Y., Aminova, L. R., Faulkner, M. J., Ho, M., & Wilson, B. A. (2012). Rho/ROCK-dependent inhibition of 3T3-L1 adipogenesis by G-protein-deamidating dermonecrotic toxins: differential regulation of Notch1, Pref1/Dlk1, and β-catenin signaling. *Frontiers in Cellular and Infection Microbiology*, *2*(June), 80. https://doi.org/10.3389/fcimb.2012.00080

Berger, E., Héraud, S., Mojallal, A., Lequeux, C., Weiss-Gayet, M., Damour, O., & Géloën, A. (2015). Pathways commonly dysregulated in mouse and human obese adipose tissue: FAT/CD36 modulates differentiation and lipogenesis. *Adipocyte*, *4*(3), 161–180. https://doi.org/10.4161/21623945.2014.987578

Cao, Z., Umek, R. M., & McKnight, S. L. (1991). Regulated expression of three C/EBP

isoforms during adipose conversion of 3T3-L1 cells. *Genes & Development*, *5*(9), 1538–1552. Retrieved from http://www.ncbi.nlm.nih.gov/pubmed/1840554

Duner, P., Al-Amily, I. M., Soni, A., Asplund, O., Safi, F., Storm, P., … Salehi, A. (2016). Adhesion G Protein-Coupled Receptor G1 (ADGRG1/GPR56) and Pancreatic beta-Cell Function. *The Journal of Clinical Endocrinology and Metabolism*, *101*(12), 4637–4645. https://doi.org/10.1210/jc.2016-1884

Eisenstein, A. (2013). G Protein-Coupled Receptors and Adipogenesis : A Focus on Adenosine Receptors, (September), 414–421. https://doi.org/10.1002/jcp.24473

Farmer, S. R. (2006). Transcriptional control of adipocyte formation. *Cell Metabolism*, *4*(4), 263–273. https://doi.org/10.1016/j.cmet.2006.07.001

Gabrielli, M., Romero, D. G., Martini, C. N., Raiger Iustman, L. J., & Vila, M. D. C. (2018). MCAM knockdown impairs PPARgamma expression and 3T3-L1 fibroblasts differentiation to adipocytes. *Molecular and Cellular Biochemistry*, *448*(1–2), 299–309. https://doi.org/10.1007/s11010-018-3334-8

Heath, V. J., Gillespie, D. A., & Crouch, D. H. (2000). Inhibition of the terminal stages of adipocyte differentiation by cMyc. *Experimental Cell Research*, *254*(1), 91–98. https://doi.org/10.1006/excr.1999.4736

Hu, E., Kim, J. B., Sarraf, P., & Spiegelman, B. M. (1996). Inhibition of adipogenesis through MAP kinase-mediated phosphorylation of PPARgamma. *Science (New York, N.Y.)*, *274*(5295), 2100–2103.

Iguchi, T., Sakata, K., Yoshizaki, K., Tago, K., Mizuno, N., & Itoh, H. (2008). Orphan G Protein-coupled Receptor GPR56 Regulates Neural Progenitor Cell Migration via a G 12/13 and Rho Pathway. *Journal of Biological Chemistry*, *283*(21), 14469–14478. https://doi.org/10.1074/jbc.M708919200

Kamiya, S., Kato, R., Wakabayashi, M., Tohyama, T., Enami, I., Ueki, M., … Fukai, F. (2002). Fibronectin peptides derived from two distinct regions stimulate adipocyte differentiation by preventing fibronectin matrix assembly. *Biochemistry*, *41*(9), 3270–3277.

Ke, N., Sundaram, R., Liu, G., Chionis, J., Fan, W., Rogers, C., … Li, Q.-X. (2007). Orphan G protein-coupled receptor GPR56 plays a role in cell transformation and tumorigenesis involving the cell adhesion pathway. *Molecular Cancer Therapeutics*, *6*(6), 1840–1850. https://doi.org/10.1158/1535-7163.MCT-07-0066

Koirala, S., Jin, Z., Piao, X., & Corfas, G. (2009). GPR56-regulated granule cell adhesion is essential for rostral cerebellar development. *The Journal of Neuroscience : The Official Journal of the Society for Neuroscience*, *29*(23), 7439–7449. https://doi.org/10.1523/JNEUROSCI.1182-09.2009

Liu, C., Huang, K., Li, G., Wang, P., Liu, C., Guo, C., … Pan, J. (2017). Ascorbic acid promotes 3T3-L1 cells adipogenesis by attenuating ERK signaling to upregulate the collagen VI. *Nutrition and Metabolism*, *14*(1), 1–12. https://doi.org/10.1186/s12986-017-0234-y

Livak, K. J., & Schmittgen, T. D. (2001). Analysis of relative gene expression data using real-time quantitative PCR and the 2(-Delta Delta C(T)) Method. *Methods (San Diego, Calif.)*, *25*(4), 402–408. https://doi.org/10.1006/meth.2001.1262

Luo, R., Jeong, S.-J., Jin, Z., Strokes, N., Li, S., & Piao, X. (2011, August 2). G protein-coupled receptor 56 and collagen III, a receptor-ligand pair, regulates cortical development and lamination. *Proceedings of the National Academy of Sciences of the United States of America*. https://doi.org/10.1073/pnas.1104821108

Luo, W., Shitaye, H., Friedman, M., Bennett, C. N., Miller, J., MacDougald, O. A., & Hankenson, K. D. (2008). Disruption of cell–matrix interactions by heparin enhances mesenchymal progenitor adipocyte differentiation. *Experimental Cell Research*,

314(18), 3382–3391. https://doi.org/10.1016/j.yexcr.2008.07.003
Mali, P., Yang, L., Esvelt, K. M., Aach, J., Guell, M., James, E., … Church, G. M. (2013). RNA-Guided Human Genome Engineering via Cas9. *Science*, *339*(6121), 823–826. https://doi.org/10.1126/science.1232033.
Mehta, P., & Piao, X. (2017). Adhesion G-protein coupled receptors and extracellular matrix proteins: Roles in myelination and glial cell development. *Developmental Dynamics*, *246*(4), 275–284. https://doi.org/10.1002/dvdy.24473
Millar, M. W., Corson, N., & Xu, L. (2018). The Adhesion G-Protein-Coupled Receptor, GPR56/ADGRG1, Inhibits Cell-Extracellular Matrix Signaling to Prevent Metastatic Melanoma Growth. *Frontiers in Oncology*, *8*(February), 8. https://doi.org/10.3389/fonc.2018.00008
Myneni, V. D., Melino, G., & Kaartinen, M. T. (2015). Transglutaminase 2--a novel inhibitor of adipogenesis. *Cell Death & Disease*, *6*, e1868. https://doi.org/10.1038/cddis.2015.238
Nobusue, H., Onishi, N., Shimizu, T., Sugihara, E., Oki, Y., Sumikawa, Y., … Kano, K. (2014). Regulation of MKL1 via actin cytoskeleton dynamics drives adipocyte differentiation. *Nature Communications*, *5*, 1–12. https://doi.org/10.1038/ncomms4368
Okamura, M., Kudo, H., Wakabayashi, K., Tanaka, T., Nonaka, A., Uchida, A., … Sakai, J. (2009). COUP-TFII acts downstream of Wnt/beta-catenin signal to silence PPARgamma gene expression and repress adipogenesis. *Proceedings of the National Academy of Sciences of the United States of America*, *106*(14), 5819–5824. https://doi.org/10.1073/pnas.0901676106
Papers, J. B. C., & Doi, M. (2007). Genetic and Pharmacological Inhibition of Rho-associated Kinase II Enhances Adipogenesis *, *282*(40), 29574–29583. https://doi.org/10.1074/jbc.M705972200
Piao, X., Hill, R. S., Bodell, A., Chang, B. S., Basel-Vanagaite, L., Straussberg, R., … Walsh, C. A. (2004). G protein-coupled receptor-dependent development of human frontal cortex. *Science (New York, N.Y.)*, *303*(5666), 2033–2036. https://doi.org/10.1126/science.1092780
Rao, T. N., Marks-Bluth, J., Sullivan, J., Gupta, M. K., Chandrakanthan, V., Fitch, S. R., … Wagers, A. J. (2015). High-level Gpr56 expression is dispensable for the maintenance and function of hematopoietic stem and progenitor cells in mice. *Stem Cell Research*, *14*(3), 307–322. https://doi.org/10.1016/j.scr.2015.02.001
Rosen, E. D., Hsu, C.-H., Wang, X., Sakai, S., Freeman, M. W., Gonzalez, F. J., & Spiegelman, B. M. (2002). C/EBPalpha induces adipogenesis through PPARgamma: a unified pathway. *Genes & Development*, *16*(1), 22–26. https://doi.org/10.1101/gad.948702
Ross, S. E., Hemati, N., Longo, K. A., Bennett, C. N., Lucas, P. C., Erickson, R. L., & MacDougald, O. A. (2000). Inhibition of Adipogenesis by Wnt Signaling. *Science*, *289*(5481), 950 LP – 953. Retrieved from http://science.sciencemag.org/content/289/5481/950.abstract
Saito, Y, Kaneda, K., Suekane, A., Ichihara, E., Nakahata, S., Yamakawa, N., … Morishita, K. (2013). Maintenance of the hematopoietic stem cell pool in bone marrow niches by EVI1-regulated GPR56. *Leukemia*, *27*(8), 1637–1649. https://doi.org/10.1038/leu.2013.75
Saito, Yusuke, & Morishita, K. (2015). Maintenance of leukemic and normal hematopoietic stem cells in bone marrow niches by EVI1-regulated GPR56. *The Japanese Journal of Clinical Hematology*, *56*(4), 375–383. https://doi.org/10.11406/rinketsu.56.375
Schroeder-Gloeckler, J. M., Rahman, S. M., Janssen, R. C., Qiao, L., Shao, J., Roper, M., … Friedman, J. E. (2007). CCAAT/enhancer-binding protein beta deletion reduces adiposity, hepatic steatosis, and diabetes in Lepr(db/db) mice. *The Journal of Biological*

Chemistry, *282*(21), 15717–15729. https://doi.org/10.1074/jbc.M701329200
Shashidhar, S., Lorente, G., Nagavarapu, U., Nelson, A., Kuo, J., Cummins, J., … Foehr, E. D. (2005). GPR56 is a GPCR that is overexpressed in gliomas and functions in tumor cell adhesion. *Oncogene*, *24*(10), 1673–1682. https://doi.org/10.1038/sj.onc.1208395
Smas, C. M., & Sul, H. S. (2015). Control of adipocyte differentiation. *Biochemical Journal*, *309*(3), 697–710. https://doi.org/10.1042/bj3090697
Spaethling, J. M., Sanchez-Alavez, M., Lee, J. H., Xia, F. C., Dueck, H., Wang, W., … Eberwine, J. (2016). Single-cell transcriptomics and functional target validation of brown adipocytes show their complex roles in metabolic homeostasis. *FASEB Journal*, *30*(1), 81–92. https://doi.org/10.1096/fj.15-273797
Stoscheck, C. M. (1990). [6] Quantitation of protein. *Methods in Enzymology*, *182*, 50–68. https://doi.org/10.1016/0076-6879(90)82008-P
Titushkin, I., Sun, S., Paul, A., & Cho, M. (2013). Control of adipogenesis by ezrin, radixin and moesin-dependent biomechanics remodeling. *Journal of Biomechanics*, *46*(3), 521–526. https://doi.org/10.1016/j.jbiomech.2012.09.027
Todaro, G. J. & Green, H. (1963). Quantitative studies of the growth of mouse embryo cells in culture and their development into established lines. *Journal of Cell Biology*, *17*, 299–313.
Tontonoz, P., Graves, R. a, Budavari, a I., Erdjument-Bromage, H., Lui, M., Hu, E., … Spiegelman, B. M. (1994). Adipocyte-specific transcription factor ARF6 is a heterodimeric complex of two nuclear hormone receptors, PPAR gamma and RXR alpha. *Nucleic Acids Research*, *22*(25), 5628–5634.
White, J. P., Wrann, C. D., Rao, R. R., Nair, S. K., Jedrychowski, M. P., You, J.-S., … Spiegelman, B. M. (2014). G protein-coupled receptor 56 regulates mechanical overload-induced muscle hypertrophy. *Proceedings of the National Academy of Sciences*, *111*(44), 15756–15761. https://doi.org/10.1073/pnas.1417898111
Xu, L., Begum, S., Hearn, J. D., & Hynes, R. O. (2006). GPR56, an atypical G protein-coupled receptor, binds tissue transglutaminase, TG2, and inhibits melanoma tumor growth and metastasis. *Proceedings of the National Academy of Sciences of the United States of America*, *103*(24), 9023–9028. https://doi.org/10.1073/pnas.0602681103

661 **Figure legends**

662 **Fig.1** *GPR*56 gene expression in rodent adipose tissue and 3T3-L1 cells. **A** Reverse-
663 transcription quantitative real-time polymerase chain reaction (QPCR) analysis of *gpr*56 gene
664 expression, normalized to *gapdh*, in lean (black bars) and obese (white bars) male Zucker rat
665 abdominal visceral white adipose tissue. Histograms are the mean gene expression ($2\Delta^{Ct}$)
666 from 6 animals (n=6). Statistical analysis shows unpaired two-tailed Student t-test of lean vs
667 obese animals, ***p≤0.001. B Shows confocal images of α-GPR56 (green) immuno-stained
668 3T3-L1 cells. Non-permeabilised and permeabilised cells are indicated by – and +
669 respectively. Control cells are stained with α-Vesicular stomatitis virus G protein epitope
670 (VSVG) isotype matched and secondary antibodies or secondary antibody only as indicated.
671 Merged images show both immuno- and DAPI (blue) stain. White size bar is either 20μm (+)
672 or 5μm (-). C Histogram showing semi-quantitative analysis of Oil Red O staining of 3T3-L1
673 cells at indicated days following induction of differentiation, n=3. Statistical analysis shows
674 one-way ANOVA and Dunnett's multiple comparisons test relative to day 0 ****p≤0.0001.
675 **D** QPCR analysis of *Gpr*56, normalized to *18*S rRNA, at indicated days following induction
676 of differentiation of 3T3-L1 cells. Histogram shows mean expression relative to gene at day
677 0, which is used as calibrator, n=3. Statistical analysis shows one-way ANOVA and
678 Dunnett's multiple comparisons test relative to day 0 **p≤0.01. All error bars show standard
679 error of mean.
680
681 **Fig.2** Gpr56 knockdown in 3T3-L1 cells. **A** Schematic representation of murine *Gpr*56
682 gene exons. Exons are indicated by rectangles and coding exons are shaded. Exon numbers
683 are indicated for exons 1, 3, 11 and 14 (Ex1, Ex3, Ex11, Ex14) only. The start codon is
684 represented by ATG and approximate target regions for DsiRNAs 1, 2 and 3 indicated by
685 grey shading. Also shown are the target sequences for guide RNA plasmid vectors pCW2 and
686 pRM4, which are located in exon 3. Protospacer adjacent motif (PAM) sequences are
687 underlined. **B** Reverse-transcription quantitative real-time polymerase chain reaction analysis
688 of *Gpr*56 gene expression in 3T3-L1 cells treated with either control S. siRNA or test G-
689 DsiRNA 2 at the indicated day of differentiation. Histograms show mean gene expression of
690 3 independent experiments normalized to *18*S rRNA relative to gene expression of *Gpr*56
691 (Gpr56F & R primers) in control S. siRNA treated cells at day 0 as calibrator. Error bars
692 show standard error of mean, n=3. Statistical analysis shows multiple t test, significance
693 determined using the Holm-Sidak method of S. siRNA vs G-DsiRNA 2 each day, ** p≤0.01,

*** p≤0.001. **C** Confocal images of α-GPR56 (green) immuno-stained permeabilized control S. siRNA and G-DsiRNA 2 treated 3T3-L1 cells. Merged images show both immuno- and DAPI (blue) stain. White size bar is 20μm.

Fig.3 Adipogenesis in Gpr56 knockdown 3T3-L1 cells using G-DsiRNA 2. **A** Semi-quantitative analysis of Oil Red O stained 3T3-L1 cells at days 0, 4 and 10 of differentiation, following treatment with or without (C) the indicated scrambled control (S. siRNA) or *Gpr*56 (G-DsiRNA2) siRNA's. Histogram is the mean value of three independent experiments and the error bars the standard error of mean. Statistical analysis shows two-way ANOVA and Dunnett's multiple comparisons test of S. siRNA vs Control (C) and G-DsiRNA 2 vs Control (C), * p≤0.05, *** p≤0.01. **B** Typical western blot of S. siRNA or G-DsiRNA2 treated cells at days 0, 4 and 10 of differentiation with the indicated antibodies. Specific proteins of the expected size are indicated by black line.

Fig.4 Partial nucleotide sequence of *Gpr*56 gene alleles in 3T3-L1 genome edited cells, using single letter code. Only sequence of the pCW2 and pRM4 gRNA target regions and adjacent protospacer adjacent motif (underlined) are shown. WT depicts the normal wildtype sequence for murine *Gpr*56. Sequence shown in bold indicates deleted nucleotides of mutant alleles. CW and RM indicates nucleotide sequence of independently cloned DNA fragments derived from *Gpr*56 with – highlighting deleted region. Sequence of eight and seven independent recombinant DNA clones derived from cell clone CW2.2.4 and RM4.2.5.5 DNA respectively are shown. * indicates regions of identity between WT and CW or RM derived DNA. In both cases sequence of two distinct alleles only are seen and the size of deletion (Δ) of each allele is shown. Below the single letter nucleotide sequence are chromatograms of DNA sequence of this region for all *Gpr*56 alleles presented.

Fig.5 Adipogenesis in *Gpr*56 genome edited 3T3-L1 cells. **A** Oil Red O stained 3T3-L1 and genome edited CW2.2.4 and RM4.2.5.5 cells at days 0, 4 and 10 semi-quantified by absorbance at 492nm. Histogram is the mean value of three independent experiments and the error bars the standard error of mean. Statistical analysis shows two-way ANOVA and Dunnett's multiple comparisons test of 3T3-L1 vs CW2.2.4 or RM4.2.5.5 for each induction day, ** p≤0.01, *** p≤0.001. **B** Typical Western blot of 3T3-L1 or RM4.2.5.5 cells at days

0, 4 and 10 of differentiation with the indicated antibodies. Specific proteins of the expected size are indicated by black line.

Fig.6 Characterisation of proliferation, adhesion and extracellular matrix gene expression in *Gpr*56 genome edited 3T3-L1 cells **A** Proliferation of the indicated cell lines over the period of days shown. Histogram shows the mean of three independent experiments, n=3. Statistical analysis shows two-way ANOVA and Dunnett's multiple comparisons test of 3T3-L1 vs either RM4.2.5.5 or CW2.2.4, * $p \leq 0.05$, ** $p \leq 0.01$, *** $p \leq 0.001$, **** $p \leq 0.0001$. **B** Crystal violet stained adherent cells for the indicated cell lines, quantified by absorbance at 570nm. Histogram shows the mean of three independent experiments, n=3. Statistical analysis shows one-way ANOVA and Dunnett's multiple comparison test of 3T3-L1 vs either RM4.2.5.5 or CW2.2.4, * $p \leq 0.05$, ** $p \leq 0.01$. **C** Reverse-transcription quantitative real-time polymerase chain reaction analysis of indicated gene expression in 3T3-L1 and RM4.2.5.5 cells at days 0 and 10 of differentiation. Histograms show mean gene expression of 3 independent experiments normalized to *18*S rRNA relative to expression of the same gene in 3T3-L1 cells at day 0 as calibrator, n=3. Statistical analysis by two-way ANOVA and Sidak's multiple comparisons test of 3T3-L1 vs RM4.2.5.5 cells for each induction day, * $p \leq 0.05$, ** $p \leq 0.01$, *** $p \leq 0.001$, **** $p \leq 0.0001$. All error bars show standard error of mean.

Fig.7 **A** Confocal images of Phalloidin staining of actin cytoskeleton in 3T3-L1 and RM4.2.5.5 cells. Actin is stained with iFlour 488 conjugated Phalloidin (green). Merged images show both Phalloidin and DAPI (blue) stain. White arrows indicate regions selected for magnification shown in adjacent panels. The white size lines indicate scale bar of 20μm or 10μm. **B** Histogram showing quantitative analysis of Phalloidin stained confocal images of the indicated cell lines using ImageJ software. Statistical analysis shows unpaired Student t test, ** $p \leq 0.01$.

Fig.8 Model illustrating adipogenesis in Gpr56 +ve and -ve cells. Model shows the cell membrane lipid bilayer and Gpr56 transmembrane protein (+ve Gpr56) indicated by a black line passing through membrane that is absent in Gpr56 -ve cells (-ve Gpr56). Chemical treatment of preadipocytes allows induction of Pparγ_2 and C/ebpα in the presence (+ve Gpr56) but not absence (-ve Gpr56) of Gpr56. Differentiation is indicated by morphological change from spindle like preadipocyte fibroblast cells to round adipocyte which occurs in the

presence of Gpr56 (indicated by solid arrow) and maintenance of the fibroblast like morphology is blocked (indicated by broken arrow). The link between Gpr56 and +ve stimulation of adipogenesis is unknown and indicated by ?. In the absence of Gpr56 the change from fibroblast to adipocyte cells is blocked (broken arrow) and cells remain fibroblast like (solid arrow). In the absence of Gpr56 several possible mechanisms are proposed to inhibit Pparγ_2/C/ebpα production (down arrow) and differentiation. Sustained levels of the known inhibitor of *Ppar*γ_2 (black line) and adipogenesis, active β-catenin, is increased (up arrow). Reduced cell proliferation, adhesion and actin cytoskeleton (down arrows) and changes in extracellular matrix (ECM) gene expression, that result from loss of Gpr56, are all proposed to contribute to inhibition of adipogenesis (indicated by broken lines).

Supplementary Figure Legends

S1 Gpr56 knockdown in 3T3-L1 cells. **A** Reverse-transcription quantitative real-time polymerase chain reaction analysis of *Gpr*56 gene expression in 3T3-L1 cells treated with the indicated DsiRNA's. Histograms show mean gene expression of 3 independent DsiRNA treated cells normalized to *18*S rRNA relative to expression of *Gpr*56 in untreated 3T3-L1 cells as calibrator, n=3. Statistical analysis shows one-way ANOVA and Dunnett's multiple comparisons test of control (C) vs DsiRNA treated cells, ** $p \leq 0.01$, **** $p \leq 0.0001$. **B** Quantitative analysis of the indicated Gpr56 immuno-stained confocal cell images using ImageJ software. Statistical analysis shows unpaired two tailed Student t test, ** $p \leq 0.01$. **C** Example of typical image of Oil Red O stained 3T3-L1 non-transfected control (NTC), scrambled siRNA (S. siRNA) and Gpr56 siRNA (DsiRNA 2) treated cells at the indicated days of differentiation. **D** Quantitative analysis of Western blot with indicated antibodies relative to REVERT™ (LiCoR) total cellular protein stain. Histograms are the mean band intensity for three independent scrambled control (S. siRNA) or *Gpr*56 siRNA (G-DsiRNA2) treated cells at days 0, 4 and 10 with the indicated antibodies, n=3. Statistical analysis shows two-way ANOVA and Sidak's multiple comparisons test of S.siRNA vs G-DsiRNA2, * $p \leq 0.05$, ** $p \leq 0.01$, **** $p \leq 0.001$. All error bars show standard error of mean.

S2 Adipogenesis of Gpr56 knockdown 3T3-L1 cells using G-DsiRNA 1. Oil Red O stained 3T3-L1 cells at days 0, 4 and 10 semi-quantified by absorbance at 492nm, following treatment with or without (C) the indicated siRNA's. Histogram is the mean value of three

independent experiments and the error bars the standard error of mean. Statistical analysis shows two-way ANOVA and Dunnett's multiple comparison test of untreated (C) vs control siRNA (S.siRNA) or untreated vs *Gpr*56 siRNA (G-DsiRNA1), (*** $p \leq 0.001$).

S3 Profile of *Ppar*γ_2 and *Ap*2 gene expression during adipogenesis of G-DsiRNA 2 treated 3T3-L1 cells. Reverse-transcription quantitative real-time polymerase chain reaction analysis of indicated gene expression in 3T3-L1 siRNA control (S.siRNA, black bars) siRNA Gpr56 (G-DsiRNA 2, white bars) treated cells using *Ppar*γ_2F, *Ppar*γ_2R, *Ap*2F and *Ap*2R primers. Histograms show mean gene expression of 3 independently transfected 3T3-L1 cells with the indicated siRNA's normalized to *18*S rRNA relative to expression of the same gene in S.siRNA treated cells at day 0 as calibrator. Error bars show standard error of mean. Statistical analysis by two-way ANOVA and Sidak's multiple comparisons test of S.siRNA vs G-DsiRNA 2 treated cells for each induction day, * $p \leq 0.05$, ** $p \leq 0.01$, *** $p \leq 0.001$.

S4 A Heteroduplex analysis of *Gpr*56 genome edited cells showing examples of second and third round clones of CW and RM cells respectively. Analytical 0.8% agarose gel electrophoresis of either uncut (U) or heteroduplex analysis (T7) of polymerase chain reaction (PCR) amplified genomic DNA from the clones indicated. The expected size bands for PCR amplified DNA of 952bp and bacteriophage T7 endonuclease digested heteroduplex DNA (approx.. 743bp or 794bp) are indicated by arrows. Selected clones CW2.2.4 and RM4.2.5.5 are indicated by *. M indicates molecular weight marker. **B** Confocal images of the indicated α-GPR56 (green) immuno-stained permeabilized cells. Control cells are stained with secondary antibody only. Merged images show both immuno- and DAPI (blue) stain. White size bar is 20μm. **C** Histogram showing quantitative analysis of images using ImageJ software. Statistical analysis shows unpaired two tailed Student t test, **** $p \leq 0.001$.

S5 A Example of typical image of Oil Red O stained 3T3-L1 and *Gpr*56 genome edited cells CW2.2.4 and RM4.2.5.5 at the indicated days (0, 4, 10) of differentiation. **B** Quantitation of regulator and marker proteins during adipogenesis of *Gpr*56 genome edited cells. Quantitative analysis of Western blot with indicated antibodies relative to REVERT™ (LiCoR) total cellular protein stain. Histograms are the mean band intensity for three independent cultures of 3T3-L1 WT and RM4.2.5.5 cells at days 0, 4 and 10 with the

indicated antibodies. Statistical analysis shows two-way ANOVA and Sidak's multiple comparisons test of 3T3L1 vs RM4.2.5.5, ** $p \leq 0.01$, *** $p \leq 0.001$.

S6 Optimisation of *β-catenin* KD and differentiation of RM4.2.5.5 cells. **A** Reverse-transcription quantitative real-time polymerase chain reaction analysis of *β-catenin* gene expression (β-catenin F & R primers) in 3T3-L1 cells treated with the indicated DsiRNA's (Mixed indicates all three DsiRNA's). Histograms show mean gene expression of 3 independent DsiRNA treated cell cultures normalized to *18*S rRNA relative to expression of *β-catenin* in untreated 3T3-L1 cells as calibrator, n=3. Statistical analysis shows one-way ANOVA and Dunnett's multiple comparisons test of control (C) vs DsiRNA treated cells, **** $p \leq 0.0001$. **B** Typical western blot of 3T3-L1 cells treated with indicated siRNA's with the indicated antibodies. Specific proteins of the expected size are indicated by black line. **C** Quantitative analysis of β-catenin WB relative to β-actin. Histograms are the mean band intensity for three independent cultures of 3T3-L1 cells treated with the indicated siRNA's. Statistical analysis shows unpaired Student t test, *** $p \leq 0.001$. **D** Oil Red O stained RM4.2.5.5 cells treated with the indicated siRNA's at days 0, 4 and 10 of differentiation, semi-quantified by absorbance at 492nm. Histogram is the mean value of three independent experiments, n=3. All error bars show standard error of mean.

Conflict of Interest Statement:

The authors have no conflicts of interest to declare

Data sharing and data accessibility:

The data that support the findings of this study are available from the corresponding author upon reasonable request.

Author contribution statement:

MAH, PR and SD performed the experimental work. MAH, CB, PEM and SP designed experiments and interpreted data. MAH and CB prepared the manuscript.

Fig.1

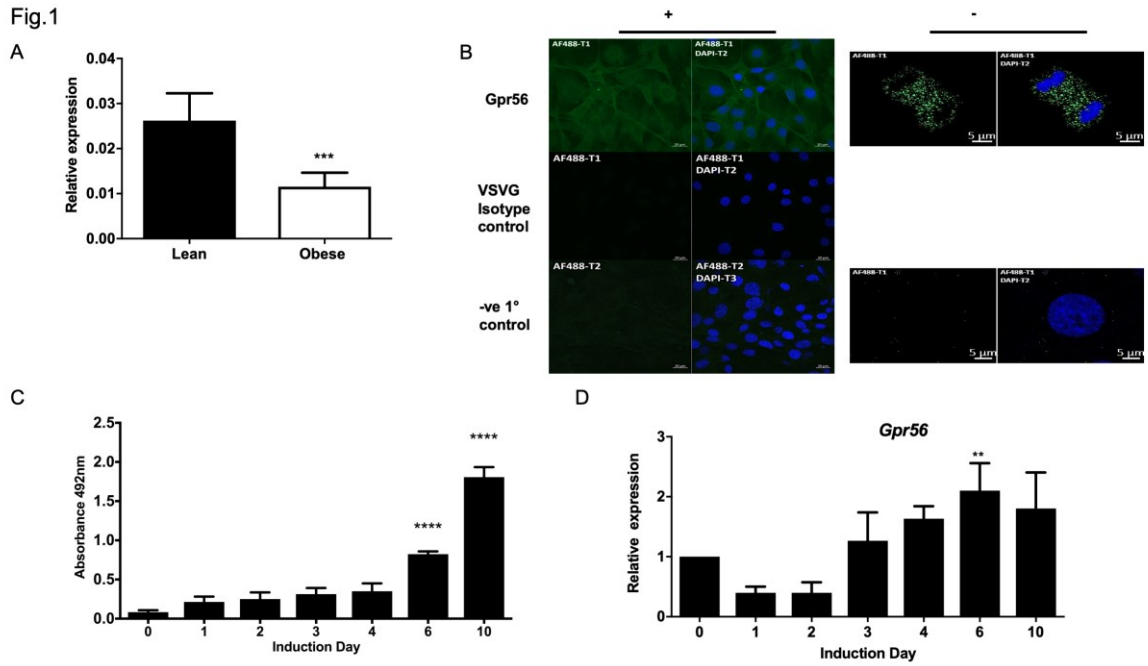

856
857

Fig.2

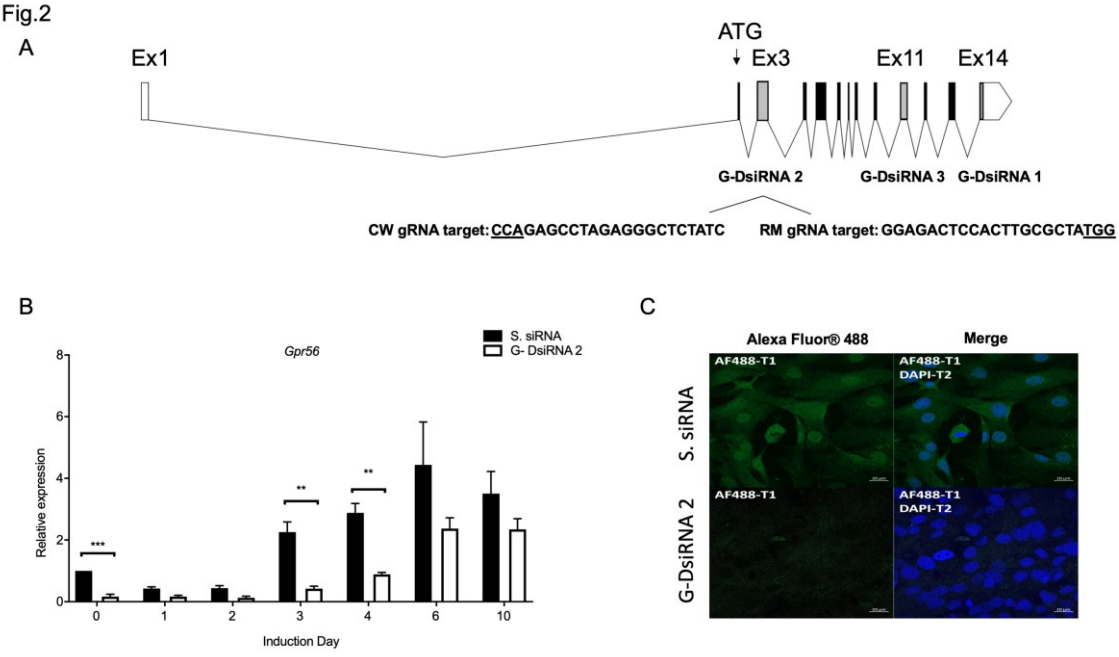

858
859

Fig.3

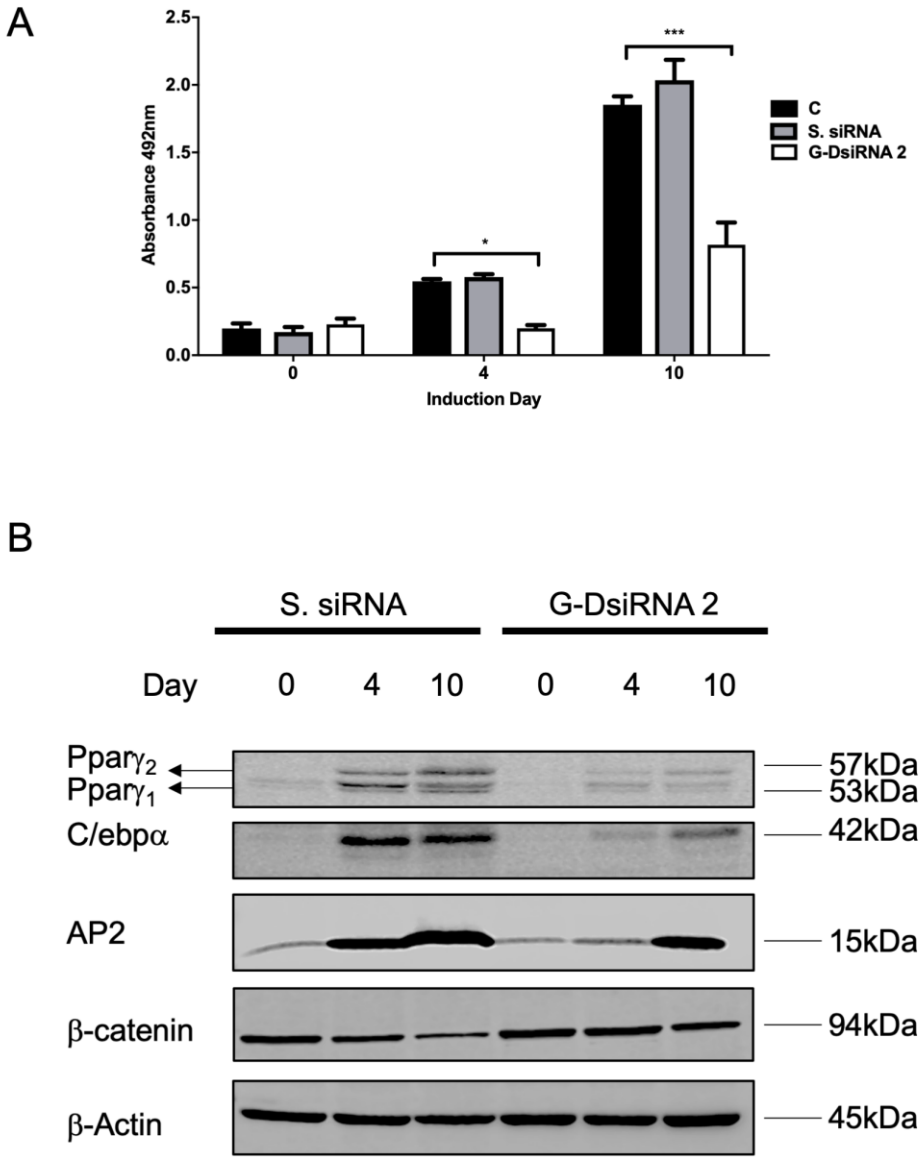
A
Absorbance 492nm
2.5
2.0
1.5
1.0
0.5
0.0
0
4
10
Induction Day
*
***
C
S. siRNA
G-DsiRNA 2
B
S. siRNA
G-DsiRNA 2
Day
0
4
10
0
4
10
Pparγ2
Pparγ1
C/ebpα
AP2
β-catenin
β-Actin
57kDa
53kDa
42kDa
15kDa
94kDa
45kDa

860
861

Fig.4

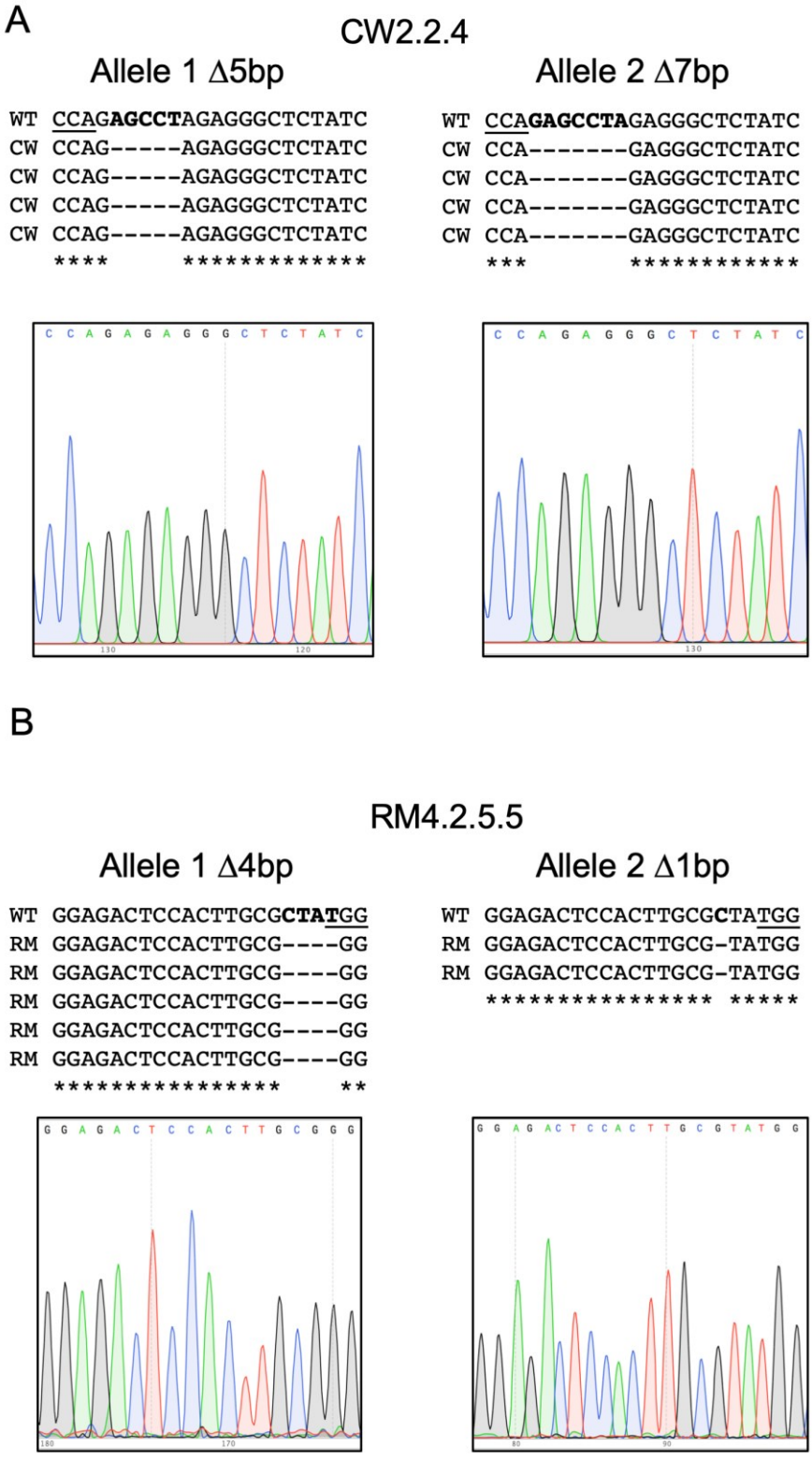
A
CW2.2.4
Allele 1 Δ5bp
Allele 2 Δ7bp
WT CCAGAGCCTAGAGGGCTCTATC
CW CCAG-----AGAGGGCTCTATC
CW CCAG-----AGAGGGCTCTATC
CW CCAG-----AGAGGGCTCTATC
CW CCAG-----AGAGGGCTCTATC
**** **********
WT CCAGAGCCTAGAGGGCTCTATC
CW CCA-------GAGGGCTCTATC
CW CCA-------GAGGGCTCTATC
CW CCA-------GAGGGCTCTATC
CW CCA-------GAGGGCTCTATC
*** **********
B
RM4.2.5.5
Allele 1 Δ4bp
Allele 2 Δ1bp
WT GGAGACTCCACTTGCGCTATGG
RM GGAGACTCCACTTGCG----GG
RM GGAGACTCCACTTGCG----GG
RM GGAGACTCCACTTGCG----GG
RM GGAGACTCCACTTGCG----GG
RM GGAGACTCCACTTGCG----GG
****
WT GGAGACTCCACTTGCGCTATGG
RM GGAGACTCCACTTGCG-TATGG
RM GGAGACTCCACTTGCG-TATGG
********** *****

862
863

Fig.5

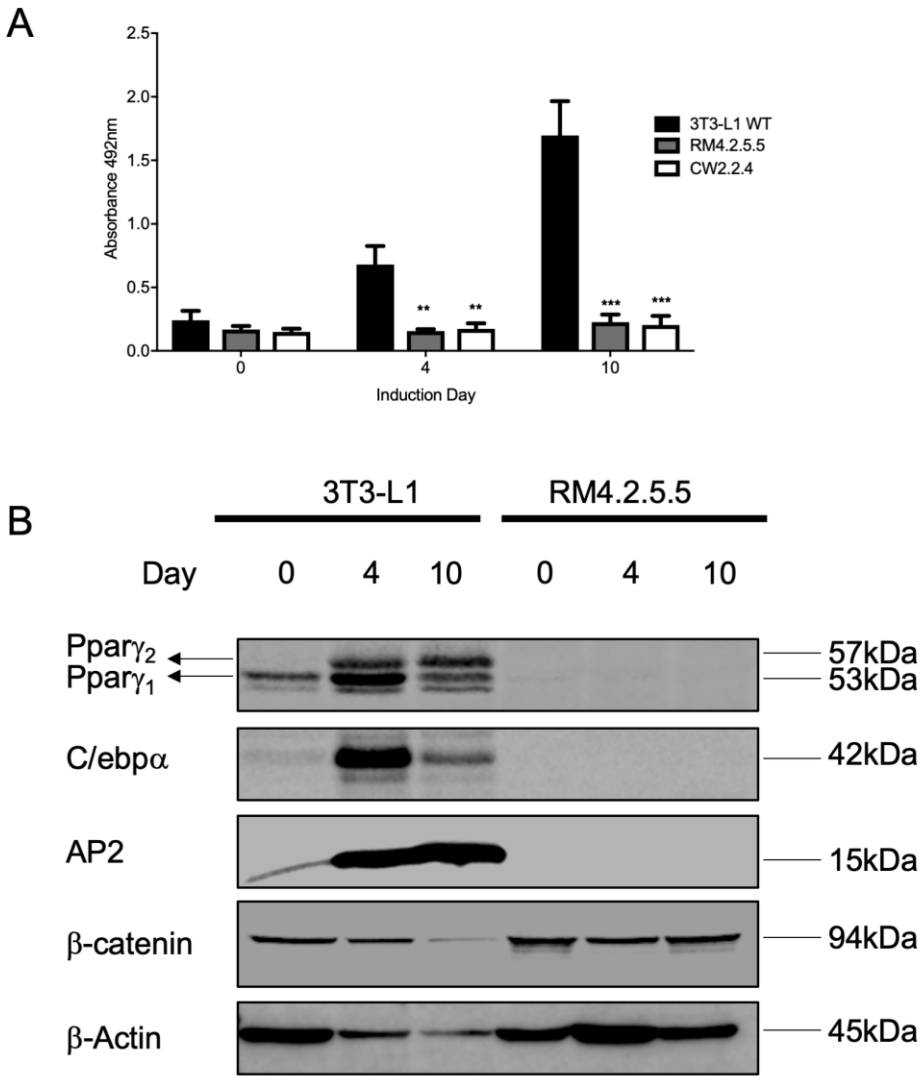
A
Absorbance 492nm
2.5
2.0
1.5
1.0
0.5
0.0
3T3-L1 WT
RM4.2.5.5
CW2.2.4
**
**
***
***
0
4
10
Induction Day
B
3T3-L1
RM4.2.5.5
Day
0
4
10
0
4
10
Pparγ2
Pparγ1
57kDa
53kDa
C/ebpα
42kDa
AP2
15kDa
β-catenin
94kDa
β-Actin
45kDa

Fig.6

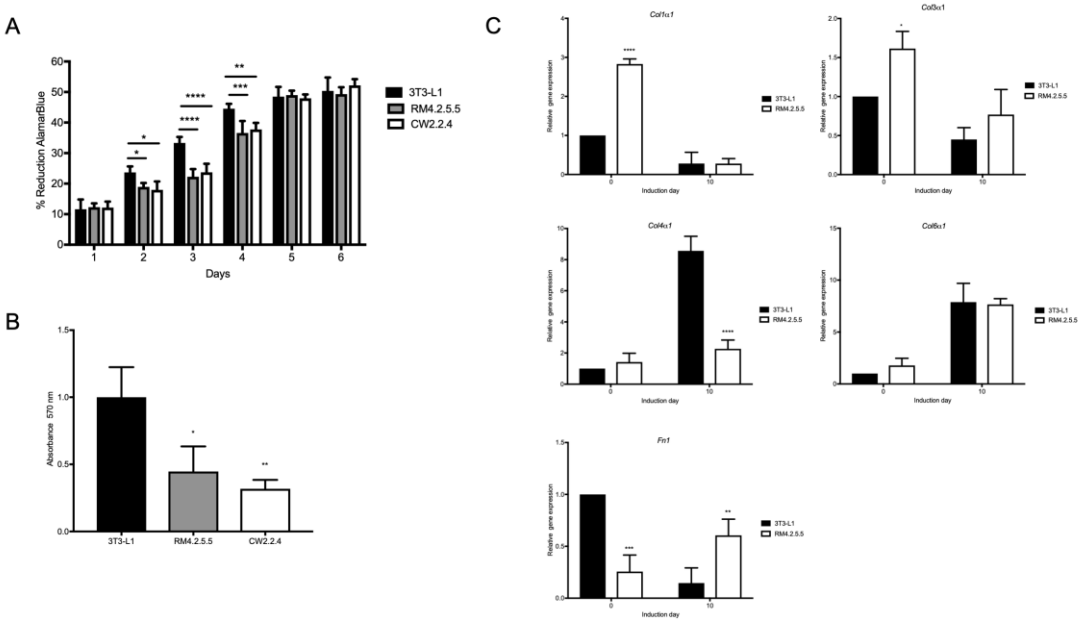
A
% Reduction AlamarBlue
Days
3T3-L1
RM4.2.5.5
CW2.2.4
B
Absorbance 570 nm
3T3-L1
RM4.2.5.5
CW2.2.4
C
Col1α1
Col3α1
Col4α1
Col6α1
Fn1
Relative gene expression
Induction day
3T3-L1
RM4.2.5.5

866
867

Fig.7

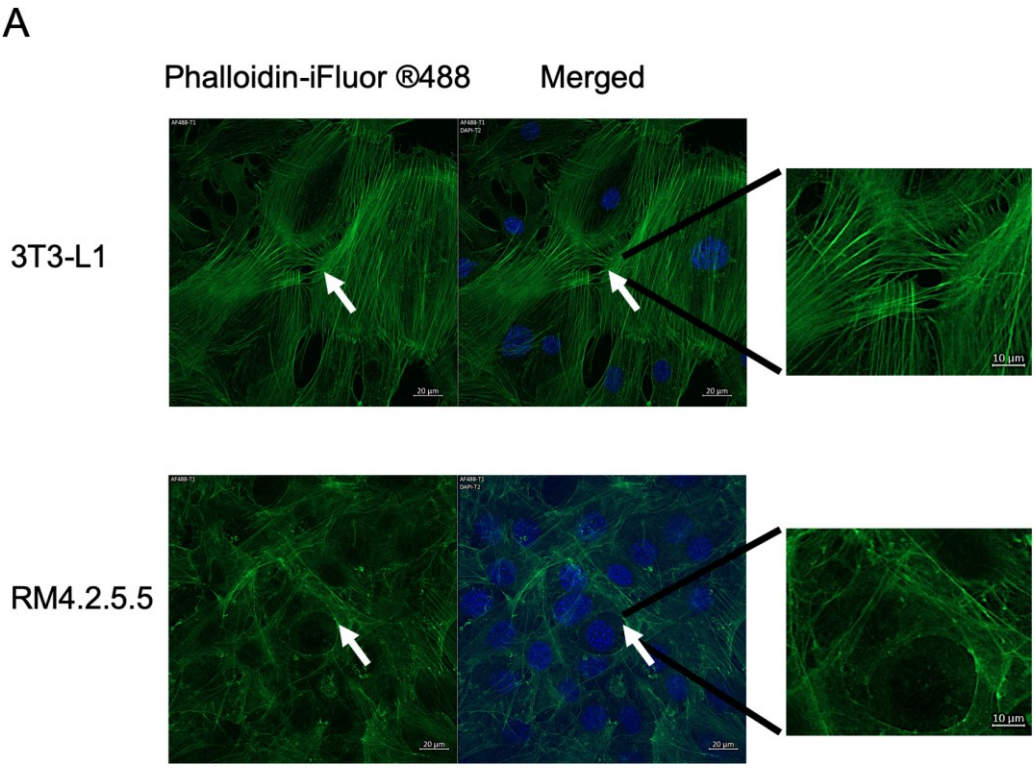
A
Phalloidin-iFluor ®488
Merged
3T3-L1
RM4.2.5.5
20 µm
10 µm

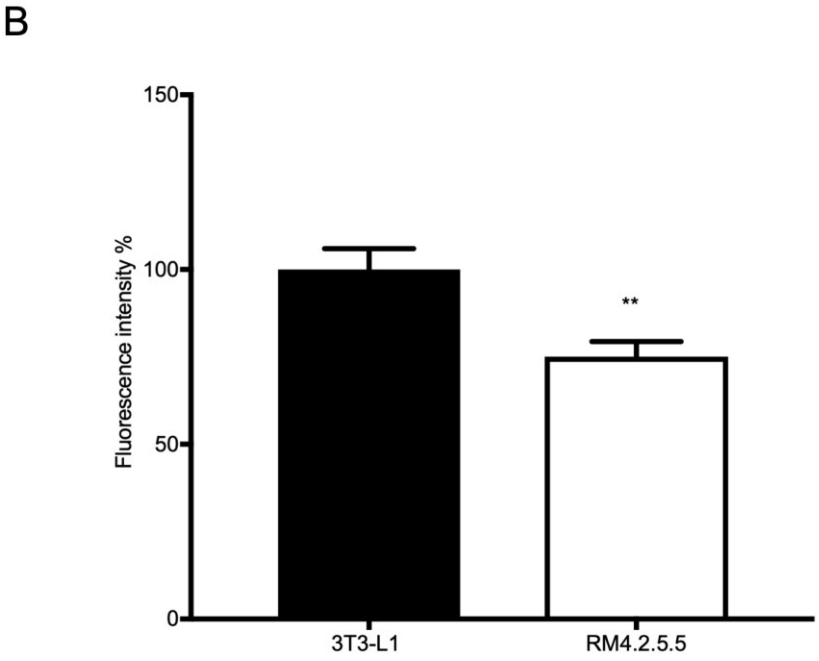
B
Fluorescence intensity %
150
100
50
0
**
3T3-L1
RM4.2.5.5

868
869

Fig.8

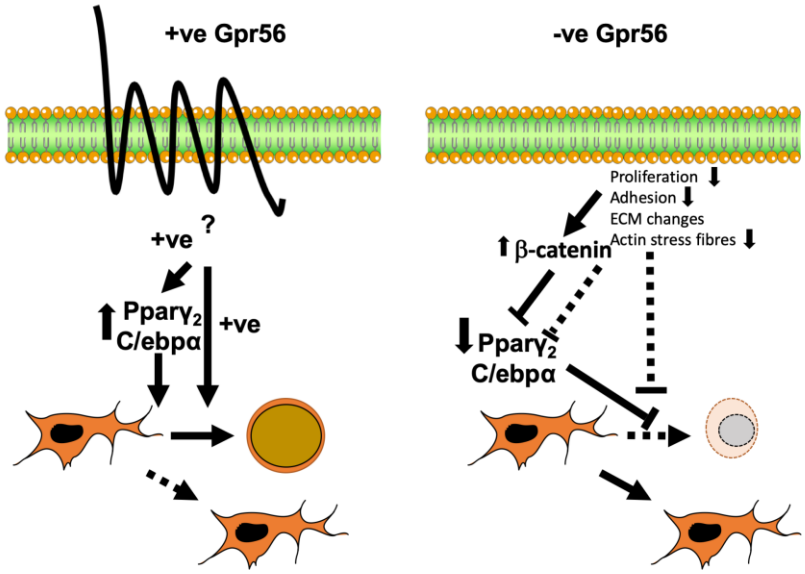
+ve Gpr56
-ve Gpr56
+ve ?
Pparγ2
C/ebpα
+ve
Proliferation
Adhesion
ECM changes
Actin stress fibres
β-catenin
Pparγ2
C/ebpα

870
871

S1

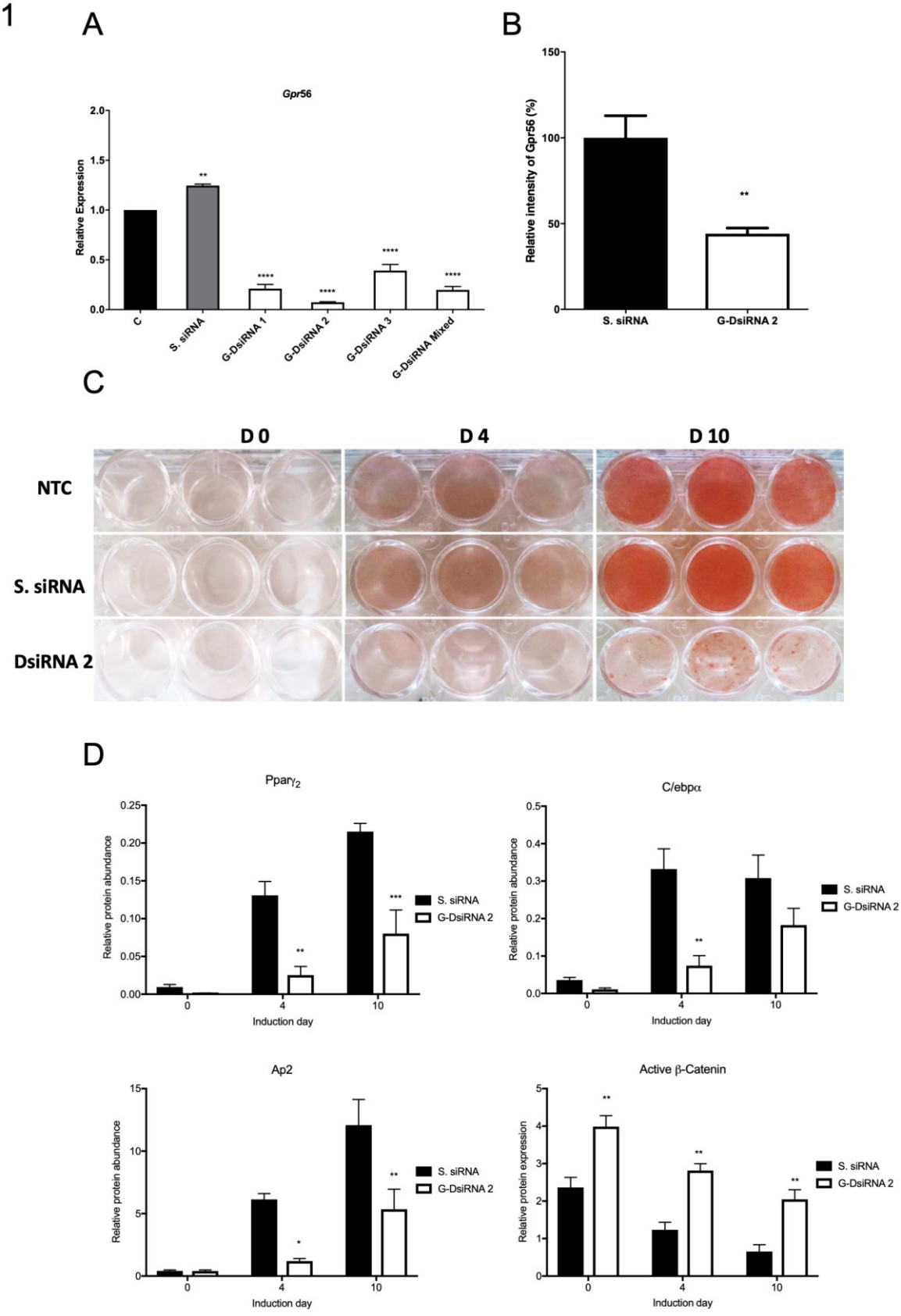
A
Gpr56
Relative Expression
2.0
1.5
1.0
0.5
0.0
**
****
****
****
****
C
S. siRNA
G-DsiRNA 1
G-DsiRNA 2
G-DsiRNA 3
G-DsiRNA Mixed
B
Relative intensity of Gpr56 (%)
150
100
50
0
**
S. siRNA
G-DsiRNA 2
C
D 0
D 4
D 10
NTC
S. siRNA
DsiRNA 2
D
Pparγ2
Relative protein abundance
0.25
0.20
0.15
0.10
0.05
0.00
**
***
0
4
10
Induction day
S. siRNA
G-DsiRNA 2
C/ebpα
Relative protein abundance
0.5
0.4
0.3
0.2
0.1
0.0
**
0
4
10
Induction day
S. siRNA
G-DsiRNA 2
Ap2
Relative protein abundance
15
10
5
0
*
**
0
4
10
Induction day
S. siRNA
G-DsiRNA 2
Active β-Catenin
Relative protein expression
5
4
3
2
1
0
**
**
**
0
4
10
Induction day
S. siRNA
G-DsiRNA 2

872
873

S2

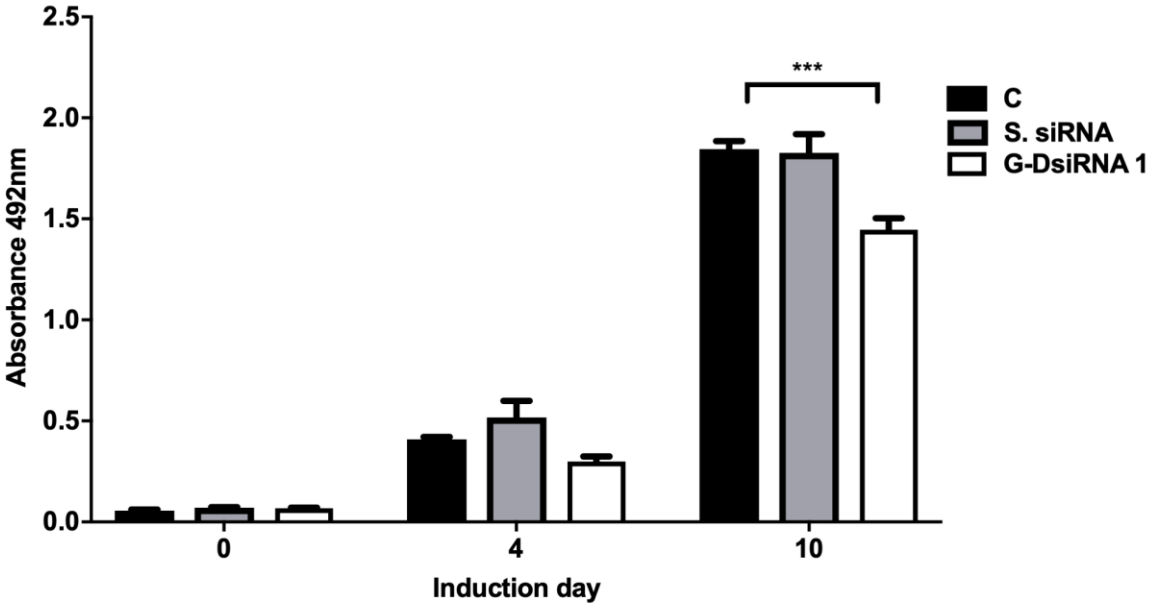
2.5
2.0
1.5
1.0
0.5
0.0
Absorbance 492nm
***
C
S. siRNA
G-DsiRNA 1
0
4
10
Induction day

874
875

S3

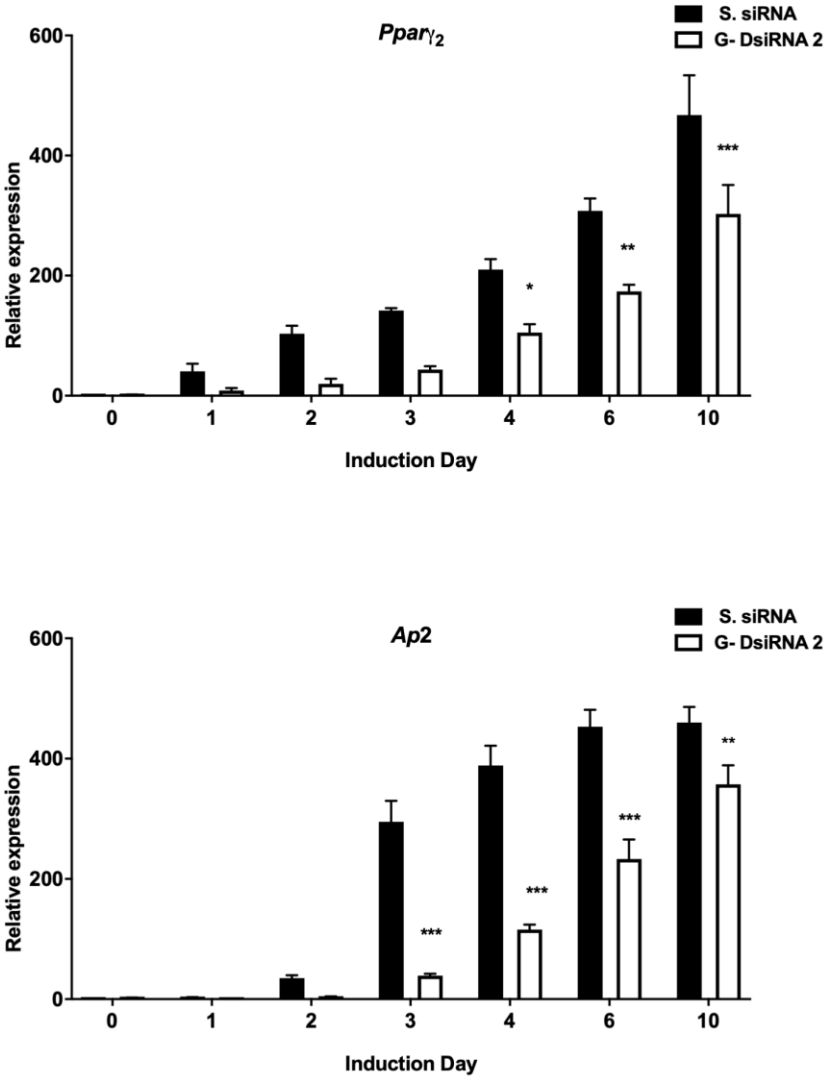
Pparγ_2
S. siRNA
G- DsiRNA 2
Relative expression
600
400
200
0
0
1
2
3
4
6
10
Induction Day
*
**
***
Ap2
S. siRNA
G- DsiRNA 2
Relative expression
600
400
200
0
0
1
2
3
4
6
10
Induction Day
***
***
***
**

876
877

S4

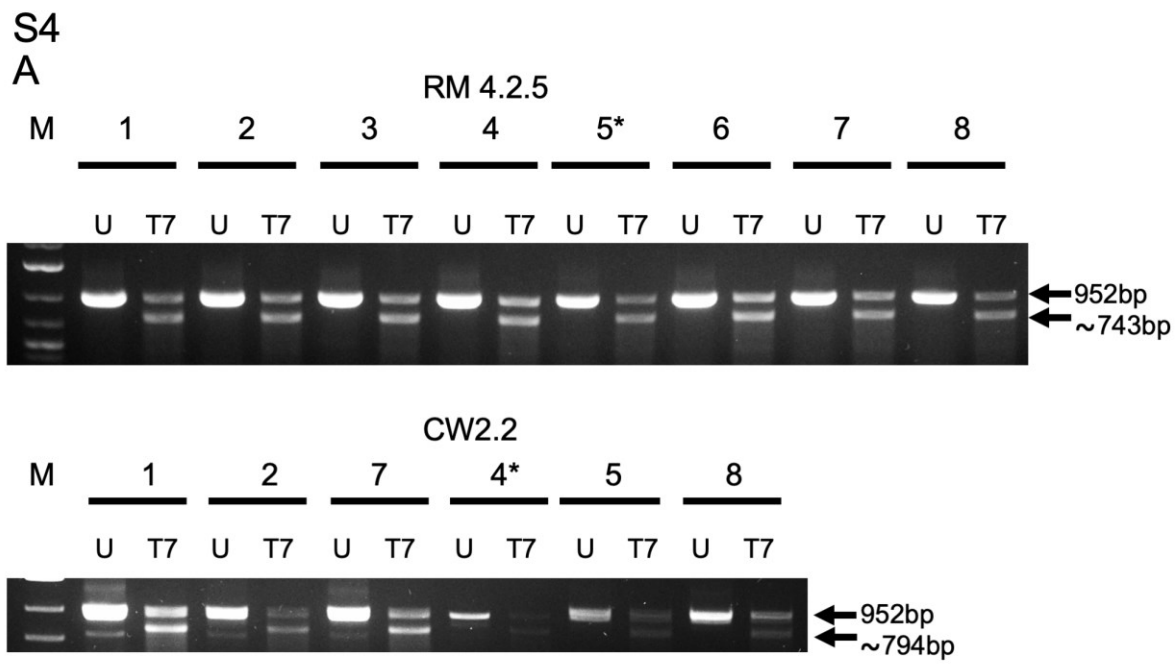
A
RM 4.2.5
M 1 2 3 4 5* 6 7 8
U T7 U T7 U T7 U T7 U T7 U T7 U T7 U T7
952bp
~743bp
CW2.2
M 1 2 7 4* 5 8
U T7 U T7 U T7 U T7 U T7 U T7
952bp
~794bp

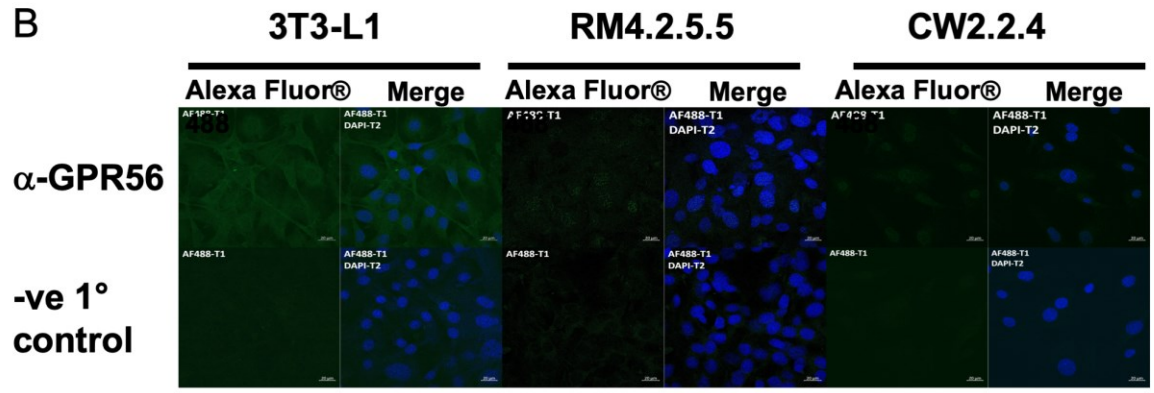
B
3T3-L1
RM4.2.5.5
CW2.2.4
Alexa Fluor®
Merge
α-GPR56
-ve 1° control
AF488-T1
DAPI-T2

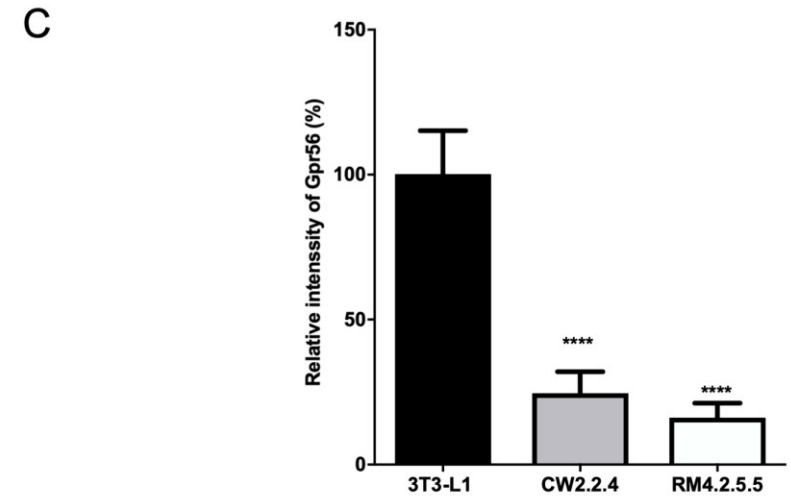
C
Relative intenssity of Gpr56 (%)
150
100
50
0
****
****
3T3-L1
CW2.2.4
RM4.2.5.5

878
879

S5

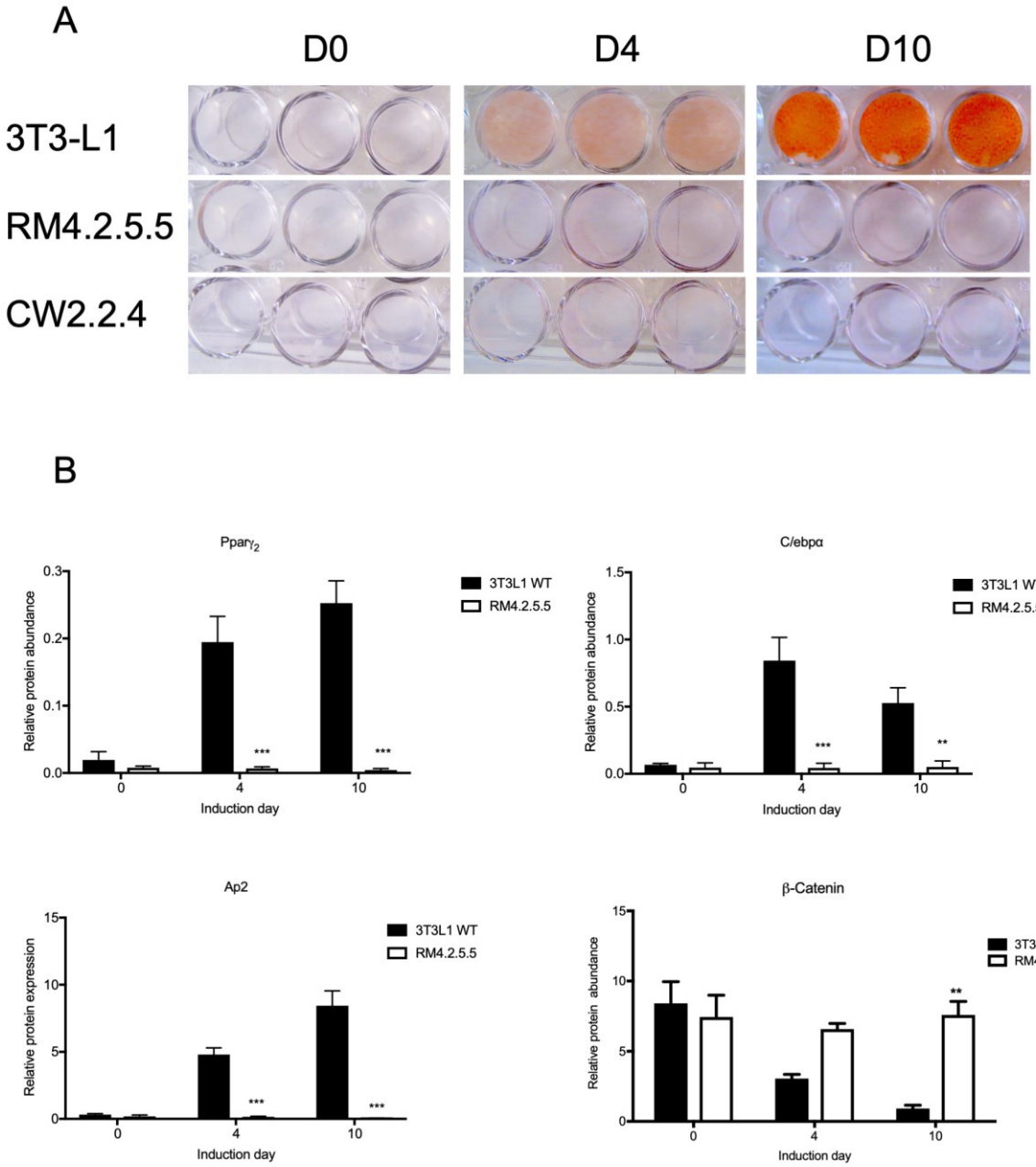
A
D0
D4
D10
3T3-L1
RM4.2.5.5
CW2.2.4
B
Pparγ2
C/ebpα
Ap2
β-Catenin
3T3L1 WT
RM4.2.5.5
3T3-L1 WT
Relative protein abundance
Relative protein expression
Induction day
0
4
10
***
**

880
881

S6

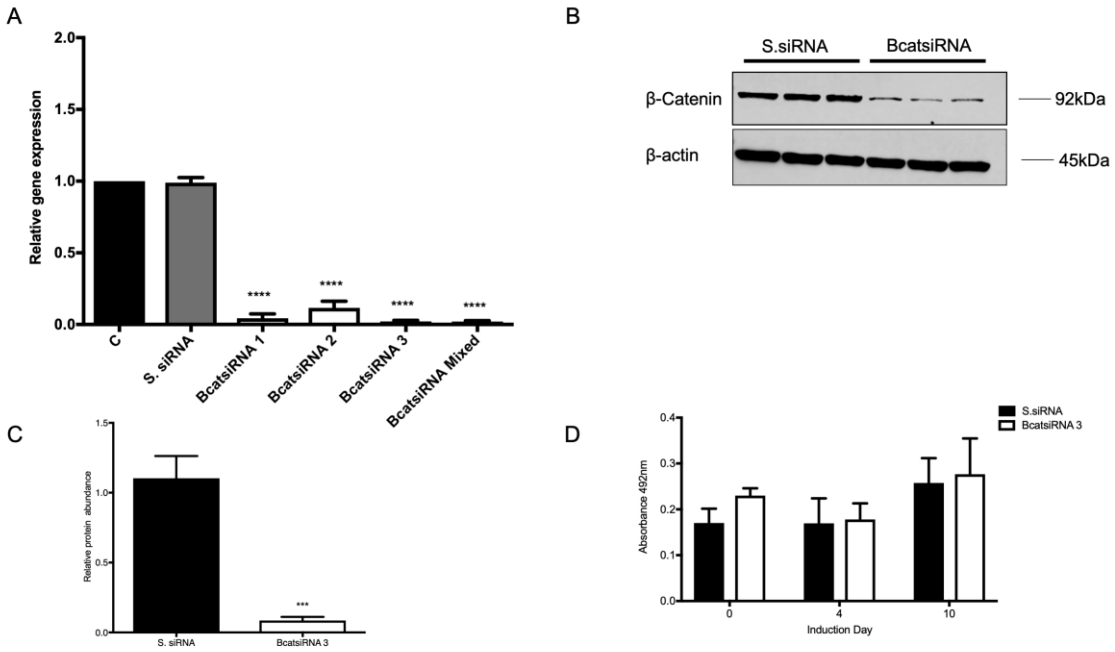
A
Relative gene expression
2.0
1.5
1.0
0.5
0.0
****
****
****
****
C
S. siRNA
BcatsiRNA 1
BcatsiRNA 2
BcatsiRNA 3
BcatsiRNA Mixed
B
S.siRNA
BcatsiRNA
β-Catenin
β-actin
92kDa
45kDa
C
Relative protein abundance
1.5
1.0
0.5
0.0
***
S. siRNA
BcatsiRNA 3
D
Absorbance 492nm
0.4
0.3
0.2
0.1
0.0
S.siRNA
BcatsiRNA 3
0
4
10
Induction Day

882